



**HAL**  
open science

## Preparation of the Experiment: Addition of Particles

Rami Alfarra, Urs Baltensperger, David M Bell, Silvia Giulia Danelli, Claudia Di Biagio, Jean-François Doussin, Paola Formenti, Martin Gysel-Beer, Dario Massabò, Gordon Mcfiggans, et al.

### ► To cite this version:

Rami Alfarra, Urs Baltensperger, David M Bell, Silvia Giulia Danelli, Claudia Di Biagio, et al.. Preparation of the Experiment: Addition of Particles. A Practical Guide to Atmospheric Simulation Chambers, Springer International Publishing; Springer International Publishing, pp.163 - 206, 2023, 10.1007/978-3-031-22277-1\_5 . hal-04192430

**HAL Id: hal-04192430**

**<https://hal.science/hal-04192430v1>**

Submitted on 31 Aug 2023

**HAL** is a multi-disciplinary open access archive for the deposit and dissemination of scientific research documents, whether they are published or not. The documents may come from teaching and research institutions in France or abroad, or from public or private research centers.

L'archive ouverte pluridisciplinaire **HAL**, est destinée au dépôt et à la diffusion de documents scientifiques de niveau recherche, publiés ou non, émanant des établissements d'enseignement et de recherche français ou étrangers, des laboratoires publics ou privés.



Distributed under a Creative Commons Attribution 4.0 International License

# Chapter 5

## Preparation of the Experiment: Addition of Particles



**Rami Alfarra, Urs Baltensperger, David M. Bell, Silvia Giulia Danelli, Claudia Di Biagio, Jean-François Doussin, Paola Formenti, Martin Gysel-Beer, Dario Massabò, Gordon McFiggans, Rob L. Modini, Ottmar Möhler, Paolo Prati, Harald Saathoff, and John Wenger**

**Abstract** Atmospheric simulation chambers are often utilized to study the physical properties and chemical reactivity of particles suspended in air. In this chapter, the various approaches employed for the addition of particles to simulation chambers are described in detail. Procedures for the generation of monodispersed seed aerosols, mineral dust, soot particles and bioaerosols are all presented using illustrative examples from chamber experiments. Technical descriptions of the methods used for the addition of whole emissions (gases and particles) from real-world sources such as wood-burning stoves, automobile engines and plants are also included, along with an outline of experimental approaches for investigating the atmospheric processing of these emissions.

### 5.1 Motivation

During the formation of secondary organic aerosol (SOA) in an atmospheric simulation chamber experiment, deposition of condensable material to the walls of the chamber can be a significant loss term when determining yields of SOA formation (Zhang et al. 2014). As a result, it is now commonplace to conduct experiments with

---

R. Alfarra · G. McFiggans  
University of Manchester, Manchester, UK

U. Baltensperger · D. M. Bell · M. Gysel-Beer · R. L. Modini  
Paul Scherrer Institute, Villigen, Switzerland

S. G. Danelli · D. Massabò · P. Prati  
Università degli Studi di Genova, Genoa, Italy

C. Di Biagio · J.-F. Doussin · P. Formenti  
Centre National de la Recherche Scientifique, Paris, France

O. Möhler · H. Saathoff  
Karlsruhe Institute of Technology, Karlsruhe, Germany

J. Wenger (✉)  
University College Cork, Cork, Ireland  
e-mail: [j.wenger@ucc.ie](mailto:j.wenger@ucc.ie)

unreactive seeds in the chamber to compete with the surfaces of the walls for the condensable material. Many aerosol generators, such as atomizers (typically used in combination with a dryer), produce high aerosol concentrations, which are suitable for out-competing walls for condensable material. Such atomizers are widely used to produce seed aerosols with a wide variety of desired chemical composition, both inorganic and organic, with varying acidity/hygroscopicity and are straightforward in their use (see, e.g. Leskinen et al. 2015; Stirnweis et al. 2017). Inorganic seeds are typically preferred because they allow for easier chemical discrimination of the seed and the formed SOA, e.g. by an aerosol mass spectrometer (AMS). The decrease in the seed aerosol concentration can also be used to correct for wall losses (Zhang et al. 2014).

A downside of the use of atomizers is that they produce rather broad particle size distributions. This results in differences in the wall loss rates for particles of different sizes (see Sect. 2.5), which can complicate the analysis of such experiments. Also, the ratio of SOA to seed aerosol mass will be different for particles of different sizes (Stirnweis et al. 2017). These difficulties can be overcome by using a classifier behind the atomizer/dryer. Such classification can be performed either based on the mobility diameter (differential mobility analyser; DMA), mass (aerosol particle mass analyser; APM) or aerodynamic diameter (aerodynamic aerosol classifier; AAC). The latter device is particularly useful as it delivers truly monomodal aerosol independent of charge distribution. All these classifiers, however, suffer from a substantial reduction in the aerosol concentration compared to the polydispersed aerosol. In the following, two techniques are described that allow for the production of higher concentrations of monodispersed seed aerosols.

### ***5.1.1 Procedure for Generation of Monodispersed Seed Aerosols***

#### **Using an electrospray atomizer**

During seeded experiments, ammonium sulphate can be generated using an electrospray aerosol generator (TSI-3480). Ammonium sulphate forms approximately spherical seed particles, which is useful when determining total water uptake based on an increase in mobility diameter. An electrospray aerosol generator can produce nearly monodisperse (geom. std. dev.  $\sigma_g = 1.3$ ) aerosol particles at concentrations that are often only achieved for polydispersed seed samples, Fig. 5.1 (Meyer et al. 2008).

#### **Aerosol generation by condensation of heated gases**

Aerosol generation by condensation of heated gases has been used in experiments conducted at the cloud chamber at CERN (Hoyle et al. 2016). Experiments were performed in a well-mixed flow chamber mode, with the sample air drawn off by the instruments continually replaced, and the mixing ratio of any added gas-phase

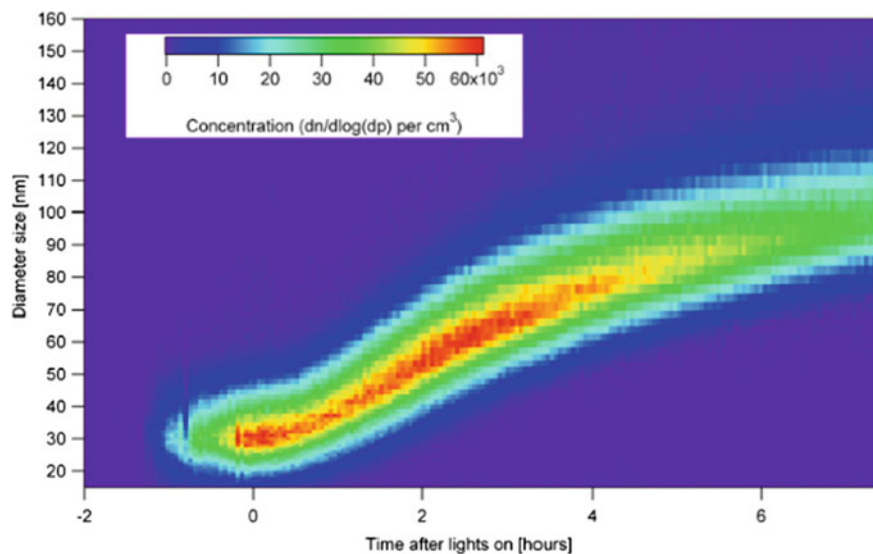


**Fig. 5.1** Time series of size distributions measured inside the chamber starting with  $(\text{NH}_4)_2\text{SO}_4$  seed aerosol (seed diameter of approximately 33 nm and  $\sigma_g = 1.3$ ) followed by the growth due to photo-oxidation of  $\alpha$ -pinene (Reused with permission from Meyer et al. (2008). Open access under a CC BY 3.0 license, <https://creativecommons.org/licenses/by/3.0/>)

species being held approximately constant. This results in a dilution lifetime of 2–3 h.  $\text{O}_3$  and  $\text{SO}_2$  were continually added to the chamber to maintain approximately constant mixing ratios, the dilution lifetime corresponds to the lifetime of the aerosol particles.

Two kinds of seed aerosol were used in these experiments, pure  $\text{H}_2\text{SO}_4$ , and partially to fully neutralized ammonium sulphate aerosol. The pure  $\text{H}_2\text{SO}_4$  aerosol was formed in an external CCN generator, which comprised a temperature-controlled stainless steel vessel holding a ceramic crucible filled with concentrated  $\text{H}_2\text{SO}_4$ . After heating the vessel to between 150 and 180 °C, depending on the desired characteristics of the aerosol population, a flow of  $\text{N}_2$  was passed through the vessel, above the crucible to transport the hot  $\text{H}_2\text{SO}_4$  vapour into the chamber. In addition, a humidified flow of  $\text{N}_2$  was added to the aerosol injection line immediately downstream of the  $\text{H}_2\text{SO}_4$  vessel, to create more reproducible size distributions. As the vapour cooled in the injection line,  $\text{H}_2\text{SO}_4$  droplets formed. The partially or fully neutralized aerosol was formed by using the same aerosol generator, and injecting  $\text{NH}_3$  directly into the chamber, where it was taken up by the acidic aerosol. The mode diameter of the aerosol distribution produced by this method was approximately 65–75 nm, with a full width at half maximum (FWHM) of approximately 50–70 nm.

In this set-up, the addition of sulphuric acid was stopped at the beginning of an experiment (to avoid the presence of particles with different ageing times. Therefore, the concentration decreased steadily by dilution of the chamber due to the instrument feed, as shown in Fig. 5.2, while the mode of the particles stayed roughly constant.

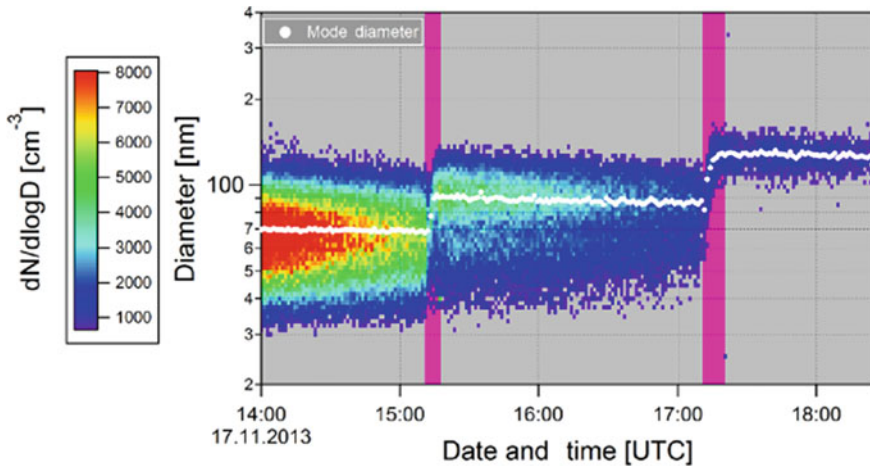


**Fig. 5.2** The aerosol size distribution measured by the scanning mobility particle sizer (SMPS) attached to the total sampling line, for a specific experiment. The white line of points shows the mode diameter. Aerosol growth is clearly observed during the cloud periods during which  $\text{SO}_2$  was taken up and transformed to sulphuric acid by ozone (marked by the purple vertical bars). (Reused with permission from Hoyle et al. (2016). Open access under a CC BY 3.0 license, <https://creativecommons.org/licenses/by/3.0/>)

## 5.2 Mineral Dust Aerosol and Its Mineral Constituents

### 5.2.1 Motivation

Mineral dust is one of the dominant aerosol species at the regional and global scales and strongly affects climate via direct and indirect radiative effects and by influencing atmospheric chemistry (Knippertz and Stuu 2014). Chamber experiments are of high relevance to elucidate the properties and processes that drive the climate impacts of mineral dust aerosols. They mostly focus on investigations of the following:

- physicochemical and spectral optical properties such as scattering, absorption, extinction cross section and complex refractive index, i.e. Linke et al. 2006; Wagner et al. 2012; Caponi et al. 2017; Di Biagio et al. 2017a, 2019);
- hygroscopicity properties (Cloud Condensation Nuclei and Ice Nuclei ability; i.e. Czico et al. 2009; Ullrich et al. 2017); and
- heterogeneous chemistry (i.e. Mogili et al. 2006; Chen et al. 2011).

In chamber studies, it is important to ensure that the laboratory-generated dust is similar in particle size, shape and composition to ambient dust aerosols, and free of contamination resulting from the generation process itself.

### 5.2.2 *Generation of Dust Aerosols from Mechanical Agitation and Vibration Devices*

These techniques involve putting a certain amount of source soil in a sample holder and then shaking or vibrating it (Lafon et al. 2014; Di Biagio et al. 2017a). Mechanical agitation or vibration provides the source material with the kinetic energy required for breaking the aggregates it contains and to generate dust aerosols which are similar to natural emissions. The mode of energy transfer for these generators is solid–solid given that the aerosols are generated from the abrasion or fracture caused when grains of the source material collide with each other and with the dust holder walls. This is the technique used recently by Utry et al. (2015), Caponi et al. (2017) and Di Biagio et al. (2014, 2017a, 2019) to study the spectral optical properties of mineral dust aerosols.

#### **Experimental procedure**

To apply the dust generation protocol described below, it is necessary to use a mechanical shaker or vibrating plate that can be regulated in frequency and amplitude. A glass sample holder with two connections (i.e. conical glass flask-type glass vacuum flask), one for the input of an inert particle-free gas and one for the dust output flow, is required. External connections are needed, i.e. from the gas supplier (gas bottle) to the sample holder (Teflon tubing) and from the sample holder to the chamber. It is recommended that the tubing connecting the sample holder to the chamber is of conductive silicone material to minimize particle loss by electrostatic deposition. There is no specific recommendation for the diameter of the tubing and connections for dust output. A general requirement is that the chamber is equipped with a ventilation system to help the aerosols to remain in suspension, in particular, the super-micron (heaviest) component. The vertical air flux from the ventilation system also allows to homogenize the distribution of the aerosol population within the chamber volume.

#### *Soil preparation*

Prior to aerosol generation, the source soil has to be:

- Dry sieved: Source soils can be used in a more or less undisturbed state as they exist in nature or they can be sieved before aerosol generation. Although soil sieving is not deemed to be essential, almost all previous studies using this generation technique have sieved the soils. In order to mimic the generation process and properties of the dust aerosols as they are in nature, a good recommendation is to sieve the soil samples at 1000  $\mu\text{m}$  in order to take into account only the fraction susceptible to erosion, so as to eliminate any non-erodable grains (Lafon et al. 2014; Di Biagio et al. 2017a).
- Dried: water vapour from the soil sample is usually removed to maximize its emission capacity, i.e. to reproduce soil conditions in source dry arid areas. To do so, samples can be heated at more than 100 °C in the oven, held in samples under vacuum, or alternatively, they can be put in a vessel partly filled with silica

gel for a few hours. If a sample shows a particular tendency to retain water, like the mineral montmorillonite, the drying process can require repeated heating and pumping cycles over a few hours or overnight pumping under vacuum conditions in order to better remove residual water (Mogili et al. 2007).

### *Material preparation*

The sample holder is cleaned and dried prior to use. The cleaning procedure may include rinsing with deionized water, 15 min of sonication, and drying under a laminar flow hood.

The silicon tubes and connections used in the system can be flushed with high-speed air to remove residual dust. If needed metallic connections can be additionally rinsed with deionized water, followed by 15 min of sonication and drying under a laminar flow hood.

### *Aerosol generation and injection*

The step-by-step procedure for dust generation is:

1. Place a few grams of soil in the sample holder and fix to the shaker or vibrating plate. The amount of soil depends on the volume of the chamber and the targeted mass or number concentration.
2. One entrance of the sample holder is connected to a source of particle-free inertial gas ( $N_2$ ) while the other is left open to laboratory air.
3. The sample holder is flushed with inertial gas for 2–3 min to eliminate gaseous impurities within the holder.
4. After flushing, the sample holder is immediately connected to the chamber port but the valve opening into the chamber is kept closed. In this way, the sample holder is closed, i.e. no contamination from ambient air will occur, and the configuration is ready for dust injection in the chamber (it will be necessary only to open the valve to make the generated dust to enter the chamber volume).
5. The shaking or vibration is activated for a few minutes. The operating frequency and amplitude of the shaking/vibration should be regulated depending on the desired number and mass concentration and size distribution of the dust. When the aerosol generation process is effective, it should be possible to see an ‘aerosol cloud’ within the sample holder. A sensitivity study based on a generation device using a shaking arm (Lafon et al. 2014) showed that shaking at a higher frequency increases the number and mass concentration of aerosol particles and also increases the ratio of the fine to coarse dust. This is because increasing the kinetic energy of the soil aggregates is known to liberate aerosols enriched in fine particles (Sow et al. 2009).
6. Dust injection in the chamber is achieved by flushing the dust aerosol suspension with a particle-free inertial gas ( $N_2$ ) while continuing to shake or vibrate the soil. The valve between the sample holder and the chamber is opened to allow the aerosol to enter the chamber. The injection typically continues for a few minutes until the desired concentration is obtained.

7. When the injection is finished, the valve connecting the sample holder to the chamber is closed and, at the same time, the inertial flow is stopped.

### Example of mineral dust aerosol generation

A picture of the system used in Di Biagio et al. (2014, 2017a, 2019) and Caponi et al. (2017) to generate dust in the 4.2 m<sup>3</sup> CESAM chamber is shown in Fig. 5.3. These studies used 15 g of soil sample sieved at 1000 μm and dried at 100 °C for about 1 h in an oven. The soil was put in a 500 ml glass vacuum flask and the vessel was flushed with N<sub>2</sub> at 10 L min<sup>-1</sup> for about 5 min to remove gaseous impurities. The soil was vibrated for 30 min at a frequency of 100 Hz by means of a sieve shaker (Retsch AS200) operated at an amplitude of 70/100. The dust suspension in the flask was injected into the CESAM chamber by flushing it with N<sub>2</sub> at 10 L min<sup>-1</sup> for about 10–15 min.

The CESAM chamber is equipped with a four-blade stainless steel fan located at the bottom of the chamber that ensures a vertical flux of approximately 10 m s<sup>-1</sup> and is used to achieve homogeneous conditions within the chamber volume (with a typical mixing time of approximately 10 min).

Figure 5.4 shows the surface size distribution of the suspended dust measured 10 min after injection in the CESAM chamber (Di Biagio et al. 2017a). Different experiments were performed with dust of various origins. Figure 5.4 shows the range of sizes measured in CESAM for experiments with Northern African samples (Tunisia, Morocco, Algeria, Libya, Mauritania, grey-shaded area) in comparison to field observations of the size distribution for dust close to source regions in Northern

**Fig. 5.3** Picture of the system used in Di Biagio et al. (2014, 2017a, 2019) and Caponi et al. (2017) to generate mineral dust aerosols. The vacuum flask is attached to the shaker using a custom-made wood plate. The Teflon white tube connecting the vessel to the N<sub>2</sub> gas bottle supplier and the black 0.64 cm silicon tube connecting it to the CESAM chamber are also visible





Africa as measured during AMMA (African Monsoon Multidisciplinary Analyses, Formenti et al. 2011), SAMUM1 (Saharan Mineral Dust Experiment, Weinzierl et al. 2009) and FENNEC (Ryder et al. 2013). The size of the generated dust in CESAM at the beginning of the experiments includes both sub- and super-micron aerosols up to more than 20  $\mu\text{m}$  in diameter and compares well with field observations. This suggests that the aerosol generation procedure is good at reproducing the size of natural dust particles measured close to the source areas.

The dust size distribution in the chamber changes significantly over time due to gravitational settling. In CESAM the lifetime of dust aerosols varies with the size. For particles smaller than 2  $\mu\text{m}$  in diameter the lifetime is  $>60$  min, but for particles larger than about 10  $\mu\text{m}$  in diameter, the lifetime is  $<10$  min (Di Biagio et al. 2017a). The rapid decrease of the coarse mode above 5  $\mu\text{m}$  is due to the much larger settling velocity of the bigger particles ( $\sim 1$   $\text{cm s}^{-1}$  at 10  $\mu\text{m}$ , compared to  $\sim 0.01$   $\text{cm s}^{-1}$  at 1  $\mu\text{m}$ ).

The range of mass concentrations obtained in CESAM during the two studies by Di Biagio et al. (2017a, 2019) was between 2 and 310  $\text{mg m}^{-3}$  at the peak of the injection. The concentration decreased to less than 1  $\text{mg m}^{-3}$  after 2 h due to the combined effects of gravitational deposition and dilution caused by instrument sampling. An example of the time evolution of dust mass concentration in CESAM is reported in Fig. 5.5 (Caponi et al. 2017).

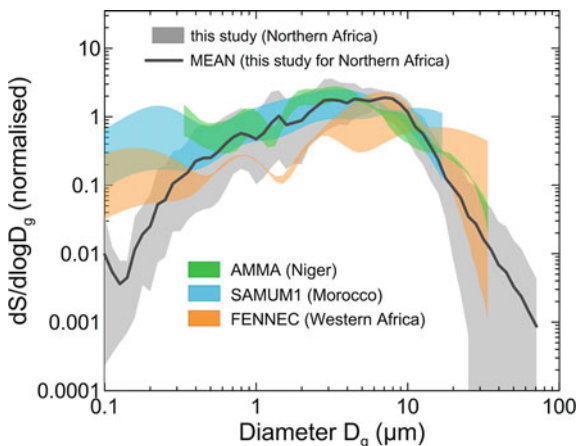


**Fig. 5.4** Surface size distribution obtained for dust aerosols from Northern Africa (Figure reused with permission from Di Biagio et al. (2017a)). Open access under a CC BY 3.0 license, <https://creativecommons.org/licenses/by/3.0/>). The grey-shaded area represents the range of sizes measured in CESAM during experiments with the different Northern African samples. Comparison of CESAM measurements at the peak of the injection with dust size distributions from several airborne field campaigns in Northern Africa is also shown. Data from field campaigns are AMMA (Formenti et al. 2011), SAMUM-1 (Weinzierl et al. 2009) and FENNEC (Ryder et al. 2013). The shaded areas for each dataset correspond to the range of variability observed for the campaigns considered

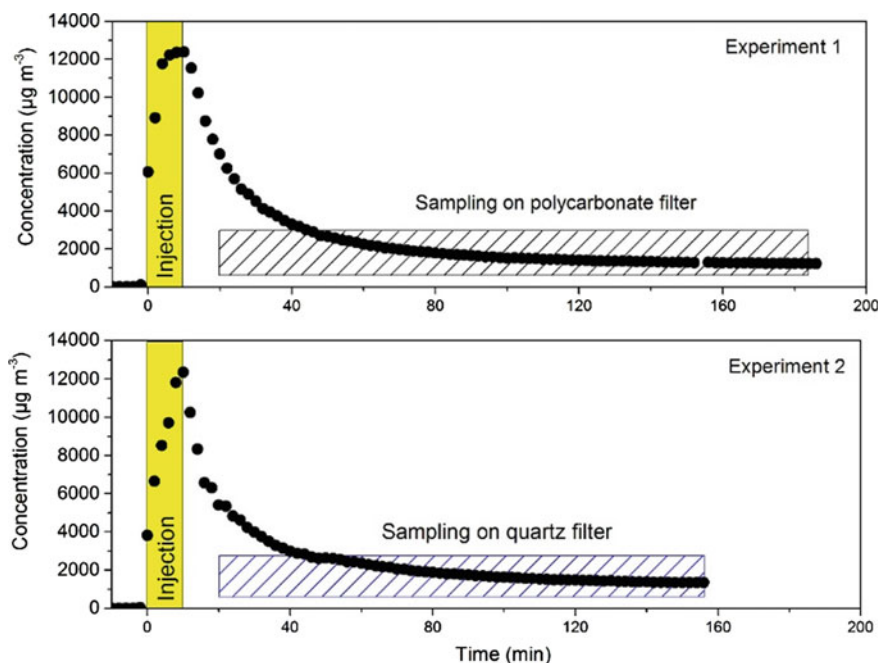


**Fig. 5.5** Time series of aerosol mass concentration in the CESAM chamber for two experiments with the same soil sample from Libya. Experiment 1 (top panel) was dedicated to the determination of the chemical composition by sampling on polycarbonate filters. Experiment 2 was dedicated to the determination of the absorption optical properties by sampling on quartz filters (Figure reused with permission from Caponi et al. (2017). Open access under a CC BY 3.0 license, <https://creativecommons.org/licenses/by/3.0/>)

Figure 5.6 shows the mineralogical composition of the dust aerosols obtained from X-Ray Diffraction analyses of particles collected on filters during experiments. The generated dust contains a wide range of silicates, calcium-rich species, feldspars and iron oxides, as expected for dust samples of varying origins. The proportions of the different minerals are also realistic compared to atmospheric dust samples, which are usually dominated by clays and quartz, with smaller amounts of calcite, dolomite, gypsum, feldspars and iron oxides (i.e. Formenti et al. 2011).

### 5.2.3 Generation of Dust Aerosols from Fluidization Devices

Fluidization devices simulate the suspension of pre-existing fine particles from a solid surface under the effect of lifting forces or drag, a process that mostly mimics the re-suspension of aerosol deposited on the ground at receptor sites. As a result, the particle size distribution of the aerosol is virtually identical to that produced when the dust is suspended in ambient air. These fluidization devices do not transfer mechanical

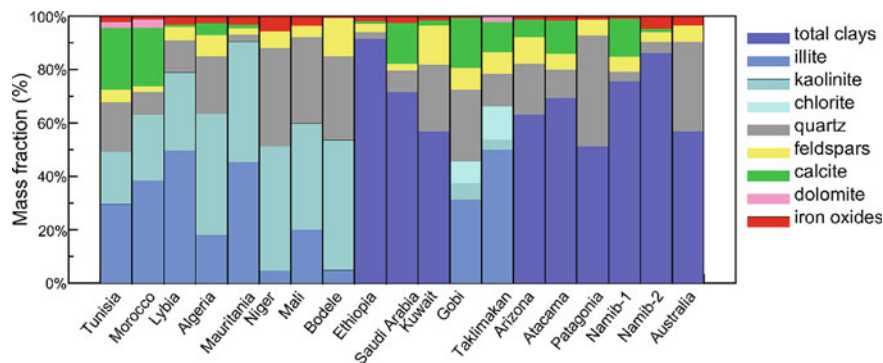


**Fig. 5.6** Mineralogical composition for nineteen dust samples with different origins investigated in CESAM (Figure reused with permission from Di Biagio et al. (2017a). Open access under a CC BY 3.0 license, <https://creativecommons.org/licenses/by/3.0/>)

or kinetic energy to dust source materials and, for this reason, they are usually referred to as ‘resuspension chambers’. Indeed, some recent fluidization devices have been designed to transfer kinetic energy to source materials with consequent de-agglomeration of soil material by the application of strong shear forces in expanding flows (nozzles) (Vlasenko et al. 2005; Linke et al. 2006; Mogili et al. 2006, 2007; Wagner et al. 2012) or by the use of high-pressure air ‘shots’ (Moosmüller et al. 2012; Engelbrecht et al. 2016). The mode of energy transfer for these generators is fluid–solid given that the energy for de-aggregating the dust agglomerates is obtained from shearing stress.

### Experimental procedure

Fluidization systems require a powder disperser and a nozzle: the disperser feeds the nozzle that de-aggregates the dust agglomerates which then enter the chamber volume. The powder disperser can be a commercial type (as in Linke et al. 2006 or Wagner et al. 2012) or custom-made (as in Mogili et al. 2006, 2007). Commercial dispersers use a rotating belt or a brush to feed dust into the injector nozzle. A custom-made system can be composed of a glass sample holder with two connections similar to the one described in 5.2.2 and a solenoid valve to put between the sample holder and the nozzle. External connections should be of conductive silicone tubing to minimize particle losses. Connections from the gas supply (gas bottle) to the powder disperser are also required (Teflon tubing). There is no specific recommendation for the diameter of the tubing and connections for dust output. A general requirement is that the chamber is equipped with a ventilation system to help the aerosols remain in suspension and to ensure their homogeneous distribution in the chamber volume.

### Soil preparation

Prior to use for aerosol generation, the source soil has to be:

Dry sieved: in all previous studies involving fluidization devices, the soils were sieved to keep only a fraction below a certain diameter (usually below 100  $\mu\text{m}$ ) for generation. The exact size may depend on the application of the specific study and the desired output size distribution. For instance, Wagner et al. (2012) sieved soils in order to keep only the fraction in the range 20–75  $\mu\text{m}$ , whereas Linke et al. (2006) sieve the soil at 20  $\mu\text{m}$  before generation.

Dried: after sieving the soil samples are dried by heating them at over 100  $^{\circ}\text{C}$  in the oven, holding them under vacuum, or putting them in a vessel partly filled with silica gel for a few hours.

### *Material preparation*

The tubing, connections and (if used) the sample holder are cleaned and dried before utilization. The cleaning procedure may include flushing with high-speed air, or rinsing with deionized water, about 10–15 min of sonication, and drying under a laminar flow hood.

### *Aerosol generation and injection*

The procedure to generate mineral dust aerosols depends on whether a commercial or custom-made disperser is used.

When a commercial disperser is used the procedure is:

1. Fill the disperser with the soil sample (typically a few to hundreds of grams of soil are required depending on the model and set-up).
2. Activate the disperser. The movement of the belt or brush in the disperser ensures a small but constant and reproducible supply of powder to the nozzle. The generated aerosol is available at the output of the nozzle. The resulting particle number concentration can be adjusted by setting the feeding belt or rotating brush speed. Particle production can be stopped without changing the gas flow through the generator by stopping the belt or brush movement.

If a custom-made disperser is used the procedure is:

1. A certain amount of soil sample is placed in the sample holder (the amount of soil will depend on the desired output concentration, but typically is a few to tens of grams).
2. One entrance of the sample holder is connected to a source of a particle-free inertial gas ( $\text{N}_2$ ) while the other is left open.
3. The sample holder is flushed with the inertial gas for 2–3 min to eliminate gaseous impurities within the holder.
4. The sample holder is pressurized to a high level with  $\text{N}_2$ .
5. The pulsed valve solenoid between the sample holder and the chamber is activated which entrains a certain amount of dispersed soil into the nozzle. The generated aerosol is available at the output of the nozzle.

Other systems are conceived so that the generation is ensured only by the use of a high-pressure air shot without the use of a nozzle (Moosmüller et al. 2012; Engelbrecht et al. 2016). In this case, the procedure is:

1. Place the soil or powder sample in a sample holder.
2. One entrance of the sample holder is connected to a source of a particle-free inertial gas ( $N_2$ ) while the other is left open.
3. The sample holder is flushed with the inertial gas for 2–3 min to eliminate gaseous impurities within the holder.

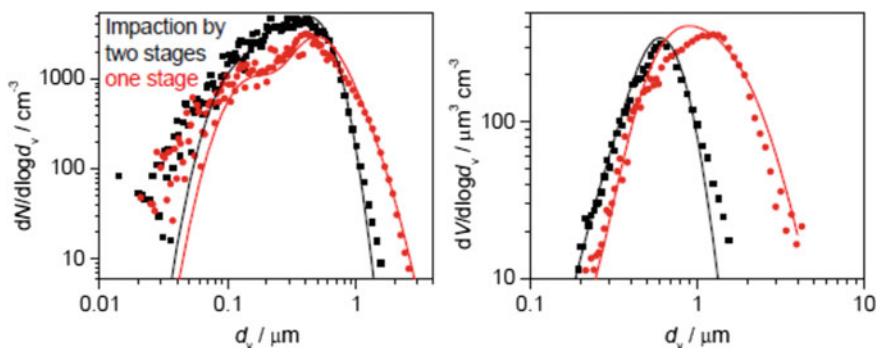
The sample holder is connected to the chamber and a pulsed high-speed jet of filtered air is injected. The air jet suspends part of the material and transports it into the chamber.

### Example of mineral dust aerosol generation

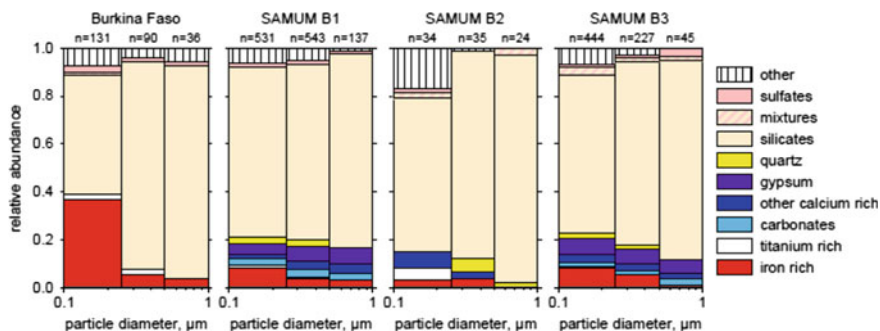
A good example of the use of this aerosol generation method is provided by Wagner et al. (2012) who generated dust aerosols to study their optical properties in the NAUA chamber ( $3.7 \text{ m}^3$ ). In this case, a commercial powder disperser (PALAS RGB 1000) was used followed by a nozzle and a cyclone system (using alternatively one or two stages) to cut the coarse particle size fraction. Both the disperser and the nozzle were operated with dry and particle-free synthetic air and the dispersion pressure of the nozzle was 1.5 bar. The resulting number and volume size distribution measured in the NAUA chamber are shown in Fig. 5.7. Because of the cyclone system, the particle cut-off size is around  $2\text{--}3 \mu\text{m}$  in diameter (two or one stages of cyclone, respectively). The initial number concentration is between  $860$  and  $6500 \text{ cm}^{-3}$ .

Figure 5.8 shows the size-resolved mineralogical composition for the four dust samples analysed by Wagner et al. (2012). The generated dust contains similar proportions of minerals as the real dust and is dominated by silicates, calcium-rich species and iron oxides as expected for the sub-micron fraction of dust.

A custom-made disperser system was used in Mogili et al. (2006, 2007) to generate aerosols from single synthetic minerals to study their extinction spectra in a  $0.151 \text{ m}^3$  environmental chamber. In their system, the mineral dust sample was put in a sample holder (conical glass flask) that was pressurized up to 100 psi (corresponding



**Fig. 5.7** Number size distribution obtained in the NAUA chamber by cutting the dust coarse fraction (Figure reused with permission from Wagner et al. (2012). Open access under a CC BY 3.0 license, <https://creativecommons.org/licenses/by/3.0/>)



**Fig. 5.8** Size-resolved mineralogical composition for four dust samples analysed in the NAUA chamber (Figure reused with permission from Wagner et al. (2012). Open access under a CC BY 3.0 license, <https://creativecommons.org/licenses/by/3.0/>)

to 6895 mbar) with a particle-free inert gas. A pulsed solenoid valve between the chamber and the sample holder was activated so that the aerosol could enter the chamber through a nozzle and an impactor plate assembly. The impactor cut-off the particles above about 2–3  $\mu\text{m}$  in diameter. The number size distribution obtained in Mogili et al. (2007) was monomodal with diameters between 107 and 357 nm. The number concentration was  $10^5$ – $10^6$   $\text{cm}^{-3}$ .

Some other studies have used fluidization devices to generate dust aerosols or their mineral components (i.e. Vlasenko et al. 2005; Linke et al. 2006; Moosmüller et al. 2012; Engelbrecht et al. 2016). In all these studies, the coarse (super-micron) dust fraction was cut by employing cyclones or impactors. The dust at the output of the nozzle or as entrained by ‘air shots’ should contain coarse mode particles; however, the aerosols were not added to simulation chambers and the size distribution was not reported.

#### 5.2.4 Generation of Dust Aerosols from Atomization of Liquid Solutions

Atomizers are widely used for studies of dust composed of single minerals (Vlasenko et al. 2006; Hudson et al. 2008a, b; Laskina et al. 2012; Di Biagio et al. 2017b). The principal drawback of this technique is that the particle size of the generated aerosols is usually confined to the accumulation mode range, with the specific diameter depending on the concentration of the solution, but usually limited to around 2.5  $\mu\text{m}$  (Hudson et al. 2008a, b).

#### Experimental procedure

The generation of aerosols using this approach involves the use of a commercial atomizer to aerosolize a suspension of dust or single minerals in ultrapure water.

The generated aerosol is usually passed through a commercial diffusion drier using inertial particle-free gas to remove water and thus dry the generated particles. Teflon and silicone tubing are routinely used in this aerosol generation procedure.

### *Soil preparation*

Prior to use for aerosol generation, the source soil can be:

Dry sieved: this procedure can be applied to keep only a fraction below a certain diameter for generation. The exact size may depend on the application of the specific study and the desired output size distribution.

### *Material preparation*

The atomizer, tubing and connections should be cleaned and dried before use. The cleaning procedure may include flushing with high-speed air, or rinsing with deionized water, about 10–15 min of sonication, and drying under a laminar flow hood.

### *Aerosol generation and injection*

Aerosol generation will consist of the following steps:

1. The sample is suspended in ultrapure water and the liquid solution is placed in the atomizer bottle.
2. The diffusion drier is connected at the output of the atomizer and the connections to the chamber are set-up.
3. The atomizer is activated by a source of inertial gas (N<sub>2</sub>) which starts the aerosolization process. Aerosols enter the chamber by opening the diffusion drier to the chamber.
4. The process is stopped when the desired concentration is achieved in the chamber.

### **Example of mineral dust aerosol generation**

Good examples of number size distributions obtained from the atomization of clays and non-clays components of mineral dust are provided by Hudson et al. (2008a, b). A solution of the minerals in Optima water (Fisher Scientific, W7-4) was atomized with a commercial atomizer (TSI Inc., Model 3076). The generated aerosols were dried to a relative humidity of 15–20% by passing through a diffusion dryer (TSI Inc., Model 3062). The resulting size distribution was shown to be mostly composed of particles <1 μm in diameter, with the peak of the number concentration located between 50 and 500 nm. The size distribution was in most cases well described by a lognormal distribution function and examples of the parameters of the lognormal functions obtained in Hudson et al. (2008a) are provided in Table 5.1. Note that the mineral samples used in the atomized solutions were ground more or less finely by Hudson et al. work. Whether ground or not, the mineral could also affect the size of the generated aerosols. By comparison, Di Biagio et al. (2017b) (not shown) used unground kaolinite mineral and generated aerosols with a larger size spectrum

**Table 5.1** Parameters of the lognormal size distribution (Median Diameter, Width) estimated for aerosols produced by atomization of clay components of mineral dust as reported in Hudson et al. (2008a)

Mineral component	Median diameter, $D_m$ (nm) <sup>a</sup>	Width, $w^a$
Illite	$153.6 \pm 2.0$	$0.88 \pm 0.01$
Kaolinite	$409.6 \pm 55.3$	$0.59 \pm 0.02$
Montmorillonite	$208.8 \pm 12.4$	$1.26 \pm 0.09$

<sup>a</sup>The lognormal function is defined here as  $y = A \exp(-\ln(D/D_m)/width)_2$

extended to the supermicron range (0.05 M solution, TSI atomizer model 3075, coupled with a diffusion drier TSI model 3062)

## 5.3 Preparation of Soot Particles for Chamber Experiments

### 5.3.1 Motivation

Soot and black carbon aerosol particles are often used as synonyms. However, this is incorrect. Black carbon (BC) is an important fraction of the carbonaceous aerosol and is characterized by its strong absorption of visible light and by its resistance to chemical transformation (Petzold et al. 2013). In the ambient atmosphere, it is formed by any incomplete combustion (e.g. gasoline or diesel exhaust, wood and coal combustion). These BC particles typically consist of agglomerates of primary spheres, which are then coated by primary organic aerosol (POA) that is co-emitted during the combustion process and condenses on the agglomerates during the cooling of the exhaust. According to the exact definition, ‘soot’ includes both the BC core material and the POA; however, it is often also used for the BC material alone. Due to the strong light absorption of black carbon, it exerts the second strongest positive radiative forcing after CO<sub>2</sub>. Despite its climatic importance, its radiative forcing is subject to a high degree of uncertainty. This is due partly not only to high uncertainties in the emission inventories but also to large variability in the mass absorption cross section (MAC). In addition, the potential of BC to act as ice nucleating particles (INP) is still under debate. Finally, BC is associated with negative health effects. Sufficient evidence has been found for an association between daily outdoor concentrations of black carbon and mortality, although the causal links have not yet been established. For these reasons, it is important to develop a better method for BC characterization in order to reduce the uncertainties related to climate impact and health effects. Chamber experiments are useful tools for BC characterization, studies of the effects of atmospheric ageing as well as its climate and health impacts.



### 5.3.2 General Approach

In these experiments, it is important to produce BC samples that are as representative as possible for the source/process under study. Some experiments use emissions from various combustion processes, such as wood combustion or car exhaust (see also Sect. 5.5 on whole emissions from real-world sources). Other experiments use lab-scale burners that produce well-controlled flames to simulate real-world combustion sources. A third type of experiment uses commercial soot samples such as AquaDAG, fullerene soot or Cab-O-Jet which are nebulized and introduced into the chamber. All three procedures are described below.

When real combustion samples are used, the soot particles do not exist of pure black carbon, but are typically coated with POA. The ratio of POA to BC as well as the properties of the BC material itself (size of the primary spherules and agglomerate size) can vary strongly with the combustion conditions (e.g. diesel soot emissions during idling or high load; flaming and smoldering conditions). Concerning the latter, Ward and Hardy (1991) define the flaming and smoldering conditions according to the modified combustion efficiency,  $MCE = CO_2 / (CO + CO_2)$ . Specifically,  $MCE > 0.9$  is identified as flaming conditions, while  $MCE < 0.85$  is identified as smoldering conditions. The actual conditions of the combustion process must therefore be described in detail for reproducible results.

The most commonly used commercial burners for simulating the production of BC are the various different miniCAST burners (Jing Ltd., Zollikofen, Switzerland, [www.sootgenerator.com](http://www.sootgenerator.com)), as well as the recently introduced miniature inverted flame soot generator (Argonaut Scientific, Edmonton, Canada). The fuel and gas flow rates in the latest versions of these burners can be adjusted precisely to produce soot particles of different sizes, concentrations and compositions (i.e. with different ratios of elemental carbon, EC, to organic carbon, OC). The latest prototype miniCAST burner (model 5201) is able to produce polydisperse soot aerosols with high EC/OC ratios over a wide range of geometric mean diameters (~50–170 nm; (Ess and Vasilatou 2019)). The Argonaut inverted burner produces polydisperse soot aerosols that peak at slightly larger diameters, up to 270 nm (Kazemimanesh et al. 2019; Moallemi et al. 2019). It is also possible to use such lab-scale burners to produce soot aerosols with high fractions of ‘organic carbon’. However, the operating conditions of these burners need to be chosen carefully to make the produced organic carbon representative of POA formed in engine exhaust (Moore et al. 2014).

When AquaDAG, fullerene soot or Cab-O-Jet samples are used, the batch number has to be specifically noted, as the properties can vary with different batches. Further details about the properties of AquaDAG and fullerene soot particles can be found in Baumgardner et al. (2012), while the properties of Cab-O-Jet particles have been reported by Zangmeister et al. (2019).

Many properties of BC particles vary with the mixing state, i.e. if particles are internally or externally mixed with other aerosol components. An example of externally mixed particles is a mixture of pure BC particles and ammonium sulphate particles. At not-too-high concentrations, the coagulation rate is relatively low, such

that the external mixture can be sustained for a few hours. An example of internally mixed particles are BC particles that are coated with secondary organic aerosol (SOA) from a gaseous precursor such as  $\alpha$ -pinene. In this case, care has to be taken to keep the concentration of the condensable SOA species sufficiently low to prevent new particle formation, which would result in a combination of external and internal mixtures.

Quantitative determination of the BC concentration is a highly challenging task. Often, absorption measurements are used, however, to retrieve a BC mass concentration the MAC value needs to be known, which can vary substantially depending on the source of the BC and its mixing state. They are therefore not treated here. EC measurements are based on quartz filter samples which undergo thermal treatment with a special protocol where the separation between EC and OC is based on their different volatility and refractoriness. During the heating step, some OC can pyrolyse at high temperature and produce extra EC, which is known as charring. This positive bias can be dealt with by correction for the attenuation of a laser signal by the extra BC, where a thermal optical reflectance (TOR) and a thermal optical transmittance (TOT) are used. In Europe, the so-called EUSAAR\_2 method is mostly used (Cavalli et al. 2010). An intercomparison has shown differences by up to a factor of 2 between these different thermal protocols (Chiappini et al. 2014; Wu et al. 2016). In addition, the limited time resolution of this method limits its application in chamber experiments.

Laser-induced incandescence (LII) has been shown to be a promising technique for the determination of refractory black carbon (rBC). The single particle soot photometer (SP2, Droplet Measurement Technologies, CO, USA) facilitates not only the measurement of the mass equivalent diameter of the rBC core but also the coating thickness of non-BC material on a single particle level (Laborde et al. 2013). Moreover, instruments applying a pulsed LII system are available. However, these instruments have mostly been used in the analysis of undiluted combustion aerosols, due to their higher detection limit, and have only recently been used in atmospheric applications.

Since no standards for rBC concentrations are available, calibration of the SP2 is best done with an aerosol particle mass analyser (APM). Using this approach, fullerene soot particles are first mass-selected followed by their rBC mass determination with an SP2. This technique has been shown to provide calibration curves that match the response of the SP2 to BC from diesel exhaust (Laborde et al. 2012a). The SP2 is a single-particle instrument capable of measuring at very high time resolution, which makes it a useful technique for detecting rapidly changing processes in chamber experiments. The main limitation of the technique is its limited detection range in terms of particle size (BC cores with individual masses between  $\sim 0.5$  and 200 fg, which corresponds to mass equivalent diameters between  $\sim 80$  and 600 nm assuming a BC material density of  $1.8 \text{ g cm}^{-3}$ ). This means, for example, that the SP2 is unable to detect small BC particles freshly emitted in diesel exhaust. In addition, at high number concentrations reported by the SP2 can be biased low due to particle coincidence in the instrument. Further details regarding the advantages and limitations of both SP2 and EC/OC measurements can be found in Pileci et al. (2021).

### 5.3.3 Procedure for Addition of Soot Particles

While several slightly different procedures have successfully been applied (see examples below), it is important to rapidly dilute the exhaust (as it also occurs in the ambient atmosphere), to avoid excessive coagulation at the high concentrations of the undiluted exhaust. To reproduce the same mixture of BC and POA as in the ambient atmosphere, the transfer into the chamber has to be performed via a heated line. If only the BC fraction is to be investigated the POA fraction can in principle be eliminated by a thermal denuder or catalytic stripper. However, it has been shown that a catalytic stripper operated at 350 °C and a residence time of 0.35 s is not able to completely eliminate all the non-refractory aerosol (Yuan et al. 2021).

Experiments with real combustion samples have been performed in various chambers. In the PSI chamber, the ageing of emissions from flaming and smoldering-dominated wood fires has been investigated in different residential stoves, across a wide range of ageing temperatures and emission loads (Bruns et al. 2015; Stefenelli et al. 2019, and references therein). At the ILMARI chamber, different anthropogenic emission sources (small-scale heaters, stoves and boilers, multifuel grate combustion reactor, passenger cars with varying fuel and after-treatment technology) have been used (see e.g. Tiitta et al. 2016). Evolution of straw biomass burning emissions was investigated in the Leipzig Biomass Burning Facility (LBBF). Experiments on the night-time chemical ageing of residential wood combustion emissions have been conducted at the ICE-FORTH environmental chamber and combustion chamber facilities. The NCAS-UMAN aerosol chamber has been coupled to a light-duty diesel engine. The combination of the collapsible 18 m<sup>3</sup> chamber design, a high flow rate clean air source (3 m<sup>3</sup>min<sup>-1</sup>) and a three-way valve enabled controlled amounts of the exhaust to be injected in the chamber allowing for a wide range of dilution ratios to be achieved (Pereira et al. 2018). These studies have enabled a focus on both the characterization of POA and the formed SOA during ageing as well as on BC mixing-state and optical properties.

While an extensive campaign was performed on BC at the AIDA chamber in 1999 with the participation of several EUROCHAMP partners (see Saathoff et al. 2003, and the whole corresponding special issue of that journal), only few studies focusing on BC were performed in the chambers of the EUROCHAMP community in more recent years. Soot emissions from a diesel engine test bench, holding a EURO-5 with a 2.0 L series Volkswagen diesel engine was used in an intercomparison study at the AIDA chamber involving six SP2 instruments, each from different research groups (Laborde et al. 2012b). It was shown that the accuracy of the SP2 mass concentration measurement depends on the calibration material chosen. In 2019, a Transnational Activity at the PSI chamber with 12 scientists from 10 different institutions was carried out, with the goal to improve reproducibility of rBC measurements using the LII technique. In these experiments, airborne AquaDAG and fullerene soot (FS) were generated by nebulizing aqueous dispersions (Collison type nebulizer; PSI home-made) followed by drying (using a silica gel-based diffusion dryer) before being injected into a steel cylinder (75 L), which served as buffer volume and, if

needed, for particle mixing. In addition, emissions from a diesel-operated, Euro 4 passenger vehicle without particle filter (Opel Combo 1.3 CDTI) were also used as BC test aerosols. The vehicle was operated only under idling conditions, and the emissions passed through a heated sampling line and dilution system before entering the chamber.

The NCAS-UMAN chamber hosted a Transnational Activity at the end of 2019, where a group of scientists from five European and North American institutions quantified the ability of a range of measurement techniques, including LII, to quantify rBC from three different sources. The research also examined the reliability of these measurements in the presence of absorbing and non-absorbing secondary organic aerosol coatings. Black carbon particles were introduced into the chamber from the following sources: (i) light-duty diesel engine (1.9 L, VW), (ii) nebulized AquaDAG and (iii) the miniature inverted flame soot generator (Argonaut Scientific, Edmonton, Canada). In one configuration of the experiments, a Catalytic Stripper (CS015; Catalytic Instruments GmbH) was used upstream of the instruments to remove the semi-volatile fraction for solid particle studies. A second configuration used a combination of a Dekati ejector dilutor, a catalytic stripper and purafil to introduce bare black carbon particles into the Manchester aerosol chamber before coating them with absorbing or non-absorbing SOA material for studies of BC optical properties.

BC particles of different O/C ratios were generated with a CAST burner, diluted and dried before injecting it into the AIDA simulation chamber for studying ice nucleation on flame soot (Möhler et al. 2005a). Information on the potential variation of OC and EC content of these soot particles is given by Schnaiter et al. (2006) and Haller et al. (2019), (Fig. 5.9).

Crawford et al. (2011) studied the heterogeneous ice nucleation on soot with different organic carbon content and with coatings of sulphuric acid. At the AIDA

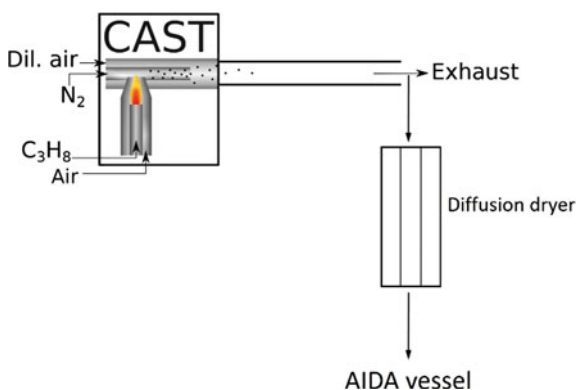


**Fig. 5.9** Combustion aerosol standard (CAST) burner for generating soot aerosol particles with different organic carbon content, depending on the C/O-ratio of the propane/ synthetic air mixture (Figure rearranged with permission from Haller et al. (2019). Open access under a CC BY 4.0 license, <https://creativecommons.org/licenses/by/4.0/>)

simulation chamber, a graphite spark generator (GfG 1000, Palas) was also used to generate model soot particles for aerosol dynamic studies (Saathoff et al. 2003) and ice nucleation studies with and without sulphuric acid coatings (Möhler et al. 2005b). Furthermore, different diesel engines on test stands were used to generate soot for the AIDA chamber, typically connected to the chamber via a denuder system optionally removing humidity, VOCs and NO<sub>x</sub> (Saathoff et al. 2003).

It is important to note that, despite recent instrumental developments, there are still considerable uncertainties in the determination of rBC or EC. Pileci et al. (2021) reported systematic discrepancies of up to  $\sim \pm 50\%$  for the sites investigated. Potential reasons for discrepancies are as follows: a source-specific SP2 response, the possible presence of an additional mode of small BC cores below the lower detection limit of the SP2, differences in the upper cut-off of the SP2 and the inlet line for the EC sampling, or various uncertainties and interferences from co-emitted species in the EC mass measurement. The lack of a traceable reference method or reference aerosols combined with uncertainties in both of the methods make it impossible to clearly quantify the sources of discrepancies or to attribute them to one or the other method, and further research is clearly warranted.

## 5.4 Bioaerosols

### 5.4.1 Motivation

Bioaerosols or Primary Biological Aerosol Particles (PBAP) such as pollen, fungal spores and bacteria can affect human health and influence the earth's climate (Després et al. 2012). Among PBAP, bacteria have a crucial role (Bowers et al. 2011). Bacterial viability, including the capability of pathogens to survive in aerosol and maintain their pathogenic potential, depends on the interaction between bacteria and the other organic and inorganic constituents in the atmospheric medium. The interactions of PBAP with other atmospheric constituents such as ozone, nitrogen oxides, volatile organic compounds, became a new, interesting topic of atmospheric science (Amato et al. 2015; Brotto et al. 2015; Massabò et al. 2018).

Atmospheric simulation chambers can provide information on the biological component of atmospheric aerosol and the interaction between bioaerosol and atmospheric conditions. Systematic experiments carried out by chambers give the opportunity to explore bioaerosol behaviour under controlled conditions. The viability of bacteria when they are dispersed in atmosphere can also be investigated, along with their correlation to air quality (Brotto et al. 2015; Massabò et al. 2018). The impact of bacteria on ice nucleation (Amato et al. 2015) is potentially important for climate and could also be relevant for spores, fungi and pollen too.

### 5.4.2 Generation of Bioaerosols from Liquid Solution

Bioaerosol studies require generators that can provide high particle concentrations with minimal damage to microorganisms. The production of a stable and viable bioaerosol is the first important element for bioaerosol research in a laboratory setting.

Currently, pneumatic nebulizers, such as collision devices, are probably the most frequently used in bioaerosol research (Alsved et al. 2019). The collision nebulizer can not only produce high concentrations of aerosol but can also cause damage to microorganisms due to recirculation of the cell suspension (Zhen et al. 2014). In recent years, several new generators have been designed for bioaerosol research, with the goal of minimizing the damage to microorganisms. Examples are the Blaustein Atomizing Modules (BLAM) and the Sparging Liquid Aerosol Generator (SLAG), both from CH TECHNOLOGIES (Thomas et al. 2011; Zhen et al. 2014). The BLAM unit is an improvement of the pneumatic nebulization without liquid recirculation, aiming to reduce the damage to bacterial culturability and structural integrity. The SLAG is a single-pass bubbling generator designed for low air pressure aerosolization of sensitive and delicate microorganisms: it implements the concept of bursting bubbles to aerosolize particles.

It is recommended to carry out all procedures in a biosafety cabinet or similar structure to ensure operator safety and to avoid contamination of the sample. According to the biosafety level of the microorganism or spore used, all necessary precautions have to be taken in order to protect the operator (attention to leaks in case of over-pressurizing the chamber). It is suggested to limit the experimental research to microorganisms with biosafety levels 1 and 2. Furthermore, the chamber must be equipped with a sterilization system such as germicidal UV lamps, in order to sterilize the entire volume before and after use. On a practical note, one essential requirement is that the chamber has a ventilation system to homogenize the distribution of the aerosol inside the volume and to help the aerosols to remain in suspension.

#### General procedure

The following equipment are required for the bioaerosol generation protocol described below:

- Teflon tube for the connection between the compressed air source and the nebulizers (typically 1/4" OD tube).
- Mass flow controller to manage the airflow.
- A syringe containing the solution to be sprayed.
- Silicon tube with Luer-lock connection to connect the syringe to the liquid inlet of BLAM or SLAG atomizer.
- A precision pump to feed the BLAM and SLAG atomizer.

It is important to note that each atomizer runs with a different pressure range and aerosolization flow rate. Each nebulizer must have its own adapter, to connect it to the chamber via a gate valve.

The procedure for operating a collision nebulizer is:

1. Connect the collision nebulizer to a source of clean, compressed air (i.e. a cylinder of dry air) with a Teflon tube, Fig. 5.10. The pressure range is 1–6 bar, which corresponds, for a 1-jet model, to an airflow rate from 2 to 7 lpm. It is recommended to use a mass flow meter or a precision pressure gauge to regulate the desired flow.
2. Position the bacteria suspension directly in the glass jar with the liquid level covering the nozzle no more than 1 cm (May 1973; Brotto et al. 2015). When the airflow is switched on, nebulization occurs immediately.

The procedure for operating a BLAM is:

1. Use a 1/4" OD tube to connect the compressed air line to the inlet of the BLAM. Use appropriate pressure and flow controllers to regulate the airflow, Fig. 5.11. The operating air pressure range is from 1 to 6 bar which gives a resulting air flow rate between 1 and 4 lpm.
2. Fill the jar with about 20–30 ml of test solution, taking care not to fill the jar excessively. The solution serves only as a soft impaction surface for the aerosol and will not be used for atomization.

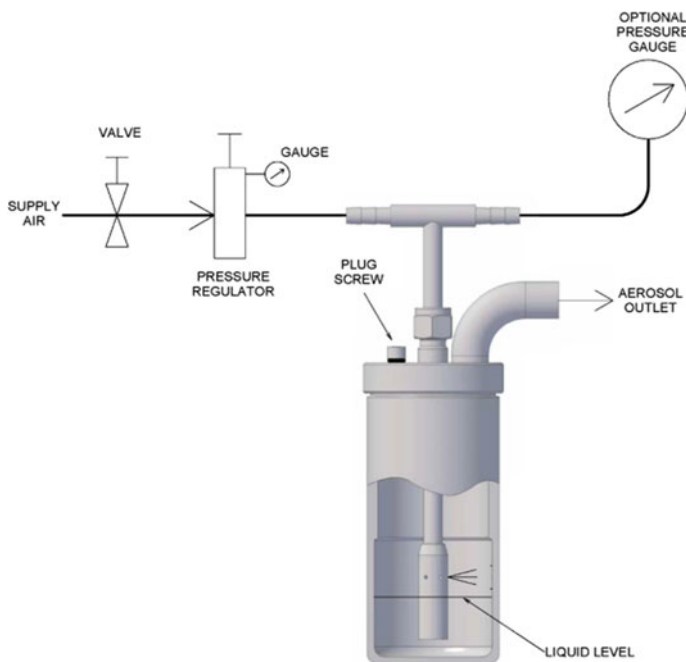


**Fig. 5.10** Schematic diagram of Collision nebulizer. Figure extracted from the nebulizer manual by CH Technologies. Collision Nebulizer—User’s Manual. Westwood, NJ, USA. [https://chtechusa.com/products\\_tag\\_lg\\_collision-nebulizer.php](https://chtechusa.com/products_tag_lg_collision-nebulizer.php)

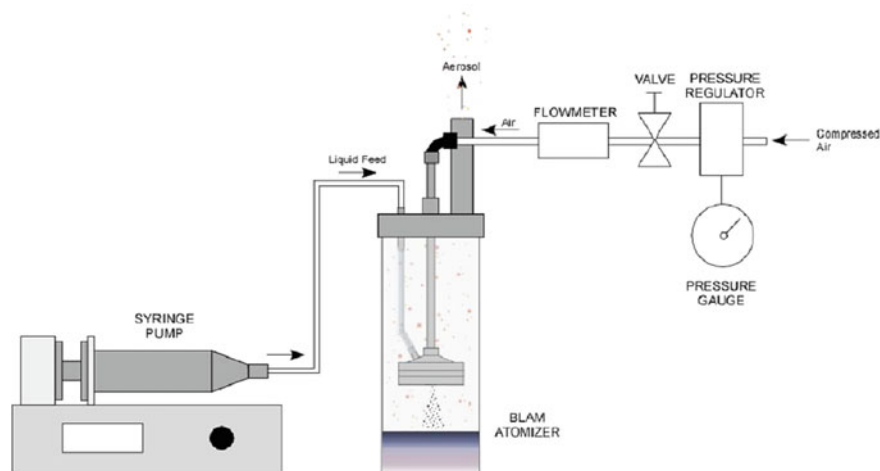


**Fig. 5.11** Schematic diagram of BLAM nebulizer. Figure extracted from CH Technologies. Blaustein Atomizer (BLAM) Multi-Jet Model—User’s Manual. Westwood, NJ, USA. [https://cht.uchusa.com/products\\_tag\\_lg\\_blaustein-atomizing-modules-blam.php](https://cht.uchusa.com/products_tag_lg_blaustein-atomizing-modules-blam.php)

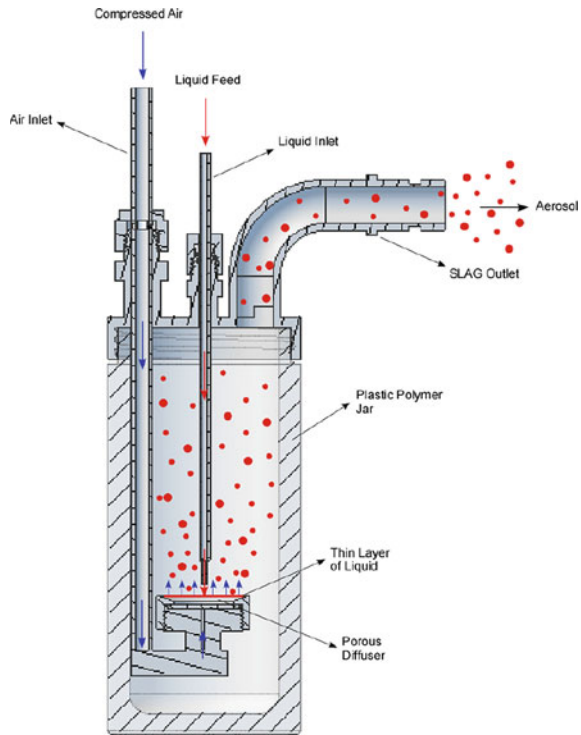
3. Use a silicon tube to connect the liquid feed port on the nozzle to the liquid feed bulkhead on the lid. Put the bacteria solution in a syringe and use a precision pump for feeding the BLAM (Liquid Feed Rate: 0.1–6 ml/min). When the liquid reaches the liquid feed port of the BLAM, turn on the compressed air supply to the device.
4. Using a mass flow controller, adjust the airflow to about 2 lpm. If a higher output is needed, increase first the upstream pressure of the compressed air line and then increase airflow rate to the atomizer (Massabò et al. 2018).
5. To stop aerosol generation, turn off the air supply to the BLAM and stop operation of the precision pump.

The procedure for operating a SLAG is:

1. Using the air pressure control instrument and a mass flow controller upstream of the SLAG, set the desired air pressure and airflow rate, Fig. 5.12. The standard SLAG model operates between 2 and 6 lpm depending on the input air pressure.
2. Use a precision pump to provide the desired liquid from a syringe filled with the bacteria solution. Use a silicon tube for the connection between the syringe and the SLAG liquid input. The optimal liquid flow rate should be such that there is all the time a thin layer of liquid on the diffuser disc surface.
3. Turn on air supply to the SLAG and in quick sequence turn on the precision pump.
4. To stop aerosol generation, simply turn off air supply to the SLAG. At the same time, stop operation of the precision pump.



**Fig. 5.12** Schematic diagram of SLAG nebulizer. Figure extracted from CH Technologies. Sparging Liquid Aerosol Generator (SLAG)—User's Manual. Westwood, NJ, USA. [https://chtechusa.com/products\\_tag\\_lg\\_sparging-liquid-aerosol-slag.php](https://chtechusa.com/products_tag_lg_sparging-liquid-aerosol-slag.php)



Typically, the injection time to have  $10^7$ – $10^8$  CFU inside the chamber is a few minutes for all nebulizers, depending on the airflow, the liquid feed rate and the desired volume to be injected. A typical value used with the BLAM and SLAG during chamber experiments is 2 ml of solution sprayed (Massabò et al. 2018). A particle counter is required to follow the injection inside the chamber. Although, it should be emphasized that if the microorganisms are suspended in physiological solution, the particle counter will mainly count the salt particles produced during the nebulization. When the injection is finished, the valve connecting the nebulizer to the chamber is closed and at the same time, the airflow and the liquid feed are stopped.

### Example of bioaerosol generation

Gram-negative bacteria *Escherichia coli* (ATCC® 25,922™) and the Gram-positive *Bacillus subtilis* (ATCC® 6633™) were selected as test bacterial species in ChAMBRe (Chamber for Aerosol Modelling and Bioaerosol Research, [www.labfisa.ge.infn.it](http://www.labfisa.ge.infn.it)). These organisms are often used in bioaerosol research as standard test bacteria (Lee et al. 2002). Prior to experiments, both the strains are cultivated on Tryptic Soy Broth (TSB) until the mid-exponential phase (Optical Density at  $\lambda = 600$  nm around 0.5) and then the bacteria are centrifuged at 4000 g for 10 min. Afterwards, bacteria are resuspended in a sterile physiological solution (NaCl 0.9%) to prepare a bacterial solution of approximately  $10^7$  CFU/ml as verified by standard

dilution plating. From this solution, 2 ml is injected inside the chamber through a flanged connection (Massabò et al. 2018). Since there are few literature available on the efficiency of nebulization of BLAM and SLAG with respect to the most used Collison nebulizer, these injection systems have been extensively characterized with typical bacterial suspensions (Danelli et al. 2021). Different airflows were tested, using a mass flow controller (Bronkhorst, model F201C-FA), to obtain the best nebulization conditions, in terms of the maximum number of viable aerosolized bacteria at the nebulizer outlet. Sampling has been carried out directly from the output of the nebulizer, through a flanged connection, using an impinging system (liquid impinger by Aquaria srl) filled with 20 mL of sterile physiological solution and operating a constant airflow of 12.5 lpm. The number of cultivable cells inside the liquid impinger was then determined as CFUs, by standard dilution plating: 100  $\mu$ L of six-fold serial dilutions of the solution was spread on an agar non-selective culture medium (trypticase soy agar, TSA), and incubated at 37 °C for 24 h before the CFU counting. Results are still to be published but, at least with *Escherichia coli* (ATCC® 25,922™), the nebulization efficiency turned out to be well reproducible and in the range of 1% for both the atomizers, with a typical ratio of 3:1 in favor of the BLAM at a fixed inlet airflow (Danelli et al. 2021). At ChAMBRé, considering the range of inlet air flows for the two devices, the typical figure for the ratio between the CFU on Petri dishes (diameter: 10 cm) placed inside the chamber to collect the bacteria by a gravitational settling and the injected CFU of *E. coli* (ATCC® 25,922™), is  $10^{-5}$  and  $10^{-6}$ , for BLAM and SLAG, respectively (Danelli et al. 2021).

The injection procedure for bacteria could be updated by adding a real-time monitor of the bioaerosol concentration inside the chamber volume, like the Wideband Integrated Bioaerosol Sensor (WIBS, University of Hertfordshire, Hertfordshire, UK, now licensed to Droplet Measurement Technologies, Longmont, CO, USA). Furthermore, even if the sequence of operations is well assessed, the need remains to tune each step to the specific bacteria strain under study. Finally, a similar but possibly different approach has to be developed for the injection of spores, fungi or pollens.

### 5.4.3 *Experimental Protocols for Studies on Fungal Spores*

Fungal spores are ubiquitous components of air in both indoor and outdoor environments. They can act as nuclei for water droplets and ice crystals, thereby potentially affecting climate and the hydrological cycle (Fröhlich-Nowoisky et al. 2009). Moreover, fungal spores in the respirable fine particle fraction ( $<3 \mu\text{m}$ ), can impact human health by triggering allergic reactions or causing infectious diseases (Kurup et al. 2000). Measurements of airborne fungal spores are typically performed offline following sampling and collection onto a range of substrates. However, recent developments in this area have seen the introduction of instruments, such as the Waveband Integrated Bioaerosol Sensor (WIBS), for online measurements of PBAP (Healy et al. 2012a).

## General procedure

Methods for the addition of various fungal spores to a small (2 m<sup>3</sup>) FEP Teflon chamber and use of the WIBS for online characterization of the BPAP have been developed by the University College Cork (Healy et al. 2012b). The general experimental set-up used for testing the addition of PBAP to the FEP Teflon chamber consists of a commercially available small-scale powder disperser (SSPD, Model 3433, TSI Inc.), a condensation particle counter (CPC, Model 3010, TSI Inc.) and a Waveband Integrated Bioaerosol Sensor (WIBS, Model 4), Fig. 5.13. All instruments were connected to the chamber using conductive tubing to minimize particle deposition. The first step in all experiments was to ensure that the chamber was cleaned and flushed with dry purified air (Zander KMA 75). The cleanliness of the chamber was checked using the CPC and deemed to be ‘clean’ if particle number concentrations were in the range of 0–50 cm<sup>-3</sup>. The relative humidity in the chamber was increased to 50–60% by gently heating a glass impinger of distilled water in a flow of purified air. The operating temperature in the chamber was in the range 293–295 K. Aerosolization of fungal spores was achieved using the SSPD. Fungal spores were gently brushed onto the surface of a pre-cleaned membrane (Nuclepore Polycarbonate, Whatman) which was subsequently attached to the rotating turntable in the SSPD. Dry purified air (Zander KMA 75) was used to flush the aerosolized spores into the chamber.

Prior to entering the WIBS, the aerosolized fungal spores were diluted at a ratio of 20:1 to safeguard against saturation of the detectors during a sample run. This was achieved using an aerosol diluter (Model 3433, TSI Inc.) and a flow rate of 4.8 l/min generated by supplementing the internal pump of the WIBS (2.4 l/min) with an auxiliary pump controlled by a flow meter, also at 2.4 l/min. The WIBS uses a 635 nm diode laser to detect particles, accompanied by two pulsed xenon UV excitation sources (280 and 370 nm) and three fluorescence detector channels (FL1, FL2 and FL3) which operate over different wavelength ranges (Healy et al. 2012b). The excitation and emission wavelengths are selected to optimize detection of the biological molecules tryptophan and nicotine adenine dinucleotide, NAD(P)H. Ultimately, for each particle, an excitation–emission matrix is recorded along with a measurement of particle size and an index of particle asymmetry, which is used to imply particle shape.

## Example of fungal spore aerosolization

The general approach outlined above was used to aerosolize the following fungal spores: *Cladosporium cladosporioides*, *Cladosporium herbarum*, *Alternaria notatum*, *Penicillium notatum* and *Aspergillus fumigatus* (Healy et al. 2012a, b). In general, all of the fungal spore samples gave higher number concentrations in the FL1 channel (Fig. 5.14), suggesting that this may be the best channel for searching for fungal spores in an ambient air. The only exception was for *Aspergillus fumigatus*, which showed similar number concentrations in the same size range for all three fluorescence channels. This observation could provide a basis for distinguishing between *Aspergillus fumigatus* and other fungal spores.

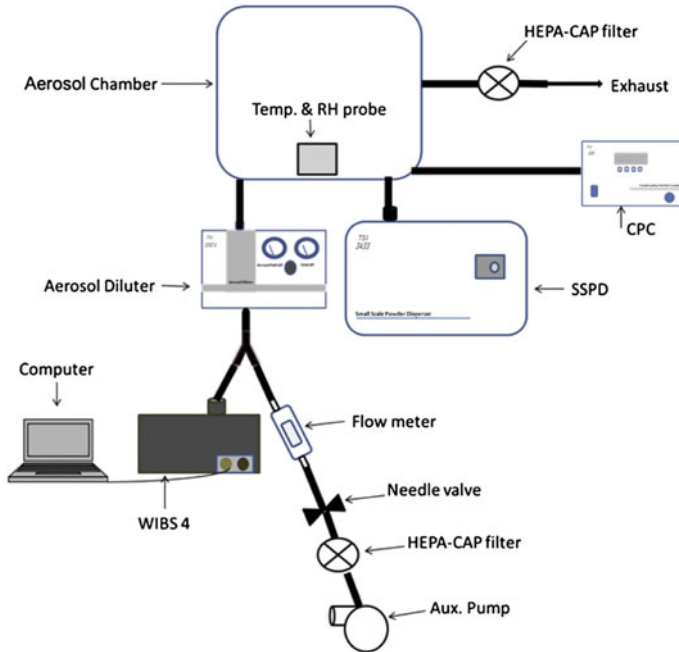


**Fig. 5.13** A schematic diagram of the experimental set-up used for the introduction of fungal spores to the FEP Teflon chamber (Healy et al. 2012b)

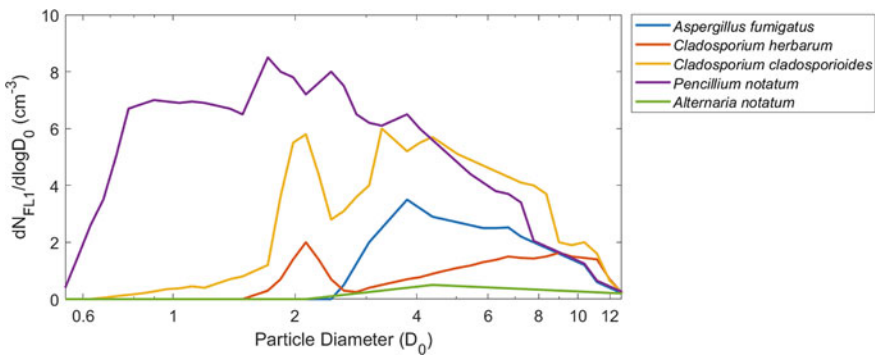


**Fig. 5.14** Particle number-size distribution profile for each type of fungal spore measured by the WIBS using fluorescent channels FL1 adapted from Healy et al, 2012b

Two of the spore types—*Pencillium notatum* and *Aspergillus fumigatus*—showed very similar profiles in all three channels. *Pencillium notatum* has by far the broadest size distribution and is the only spore type that reaches the sub-micron range. *Aspergillus fumigatus* particles are not only observed above 2.5 μm but also have a size distribution that stretches out to 12 μm. These results are in good agreement

with the aerodynamic diameters previously reported for these fungal spore types (Baron and Kulkarni 2005). The other fungal spore types show broad distributions in the FL2 and FL3 channels ranging from ca. 3–12  $\mu\text{m}$ , but in the FL1 channel, a pronounced peak at around 2  $\mu\text{m}$  was observed for both *Cladosporium cladosporioides* and *Cladosporium herbarum*. This feature indicates the clear importance of tryptophan in these fungal species and may prove to be another useful distinguishing feature when analysing field data.

The lifetime of the BPAP in the chamber was also investigated in these tests. In all cases, particle number concentrations were found to depend strongly on particle size, resulting in lifetimes ranging from 10 min for larger particles (up to 10  $\mu\text{m}$ ) to 3 h for some of the smaller *Penicillium notatum* spores. However, these measurements were subject to a high degree of variability and it is likely that electrostatic effects associated with the FEP Teflon chamber play an important role in influencing particle deposition rates (Wang et al. 2018).

## 5.5 Whole Emissions (Gases and Particles) from Real-World Sources

### 5.5.1 Motivation

Due to the importance of volatile organic compounds (VOCs) for atmospheric chemistry and gaps remaining in process-level understanding, both anthropogenic (AVOCs) and biogenic VOCs (BVOCs) and their oxidation processes are the subjects of continuous research. Atmospheric evolution of both AVOCs and BVOCs is often studied using mixtures of standard compounds that are meant to represent typical compounds from each source. In reality, AVOCs and BVOCs are emitted as complex mixtures and the detailed composition depends greatly on the source. Hence, to increase the realism and relevance of the atmospheric simulation chamber studies, measurements using real anthropogenic and biogenic sources are needed. This section will outline the best practices and methodology for coupling whole emissions from combustion sources and biogenic sources with the atmospheric simulation chamber.

### 5.5.2 Combustion Sources

One difficulty when using real combustion sources is the complexity of varying emission sources, which includes a complicated mixture of VOCs, oxidants (e.g. high concentrations of  $\text{NO}_x$ ), sulphur oxides, CO and  $\text{CO}_2$  and water vapour. The concentration of different constituents in the emissions is highly dependent on a number of parameters (e.g. combustion source, operating conditions, type of fuel,

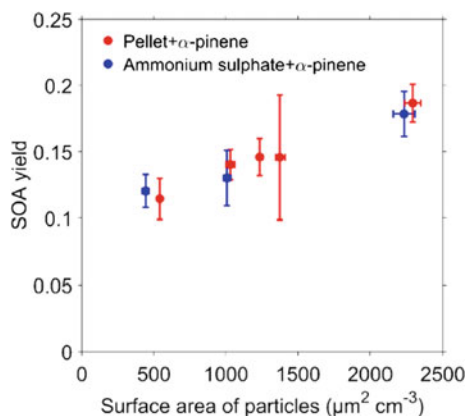
etc.). Further complicating matters, the oxidation conditions, VOC-to-NO<sub>x</sub> ratios, primary particle concentration to VOC concentration are not easily controllable. In ideal experiments, each of these parameters may be carefully chosen and injected into the chamber. For example, when SOA yields are studied, it is necessary to consider the primary particle concentration in a set of experiments because they will act as seed particles, Fig. 5.15. When using emissions from a real-world source both particulate emissions and gaseous concentrations will vary, making it difficult to prepare a chamber study for a specific source in a reproducible way. As a result, setting a precise ratio between the initial particle concentration and different concentrations of gaseous compounds is difficult.

### Wood combustion

In wood combustion studies, the feeding time of the exhaust can be varied so that the desired concentrations in the simulation chamber are achieved. Since the emission characteristics in batch combustion of wood may change remarkably during evolution of the combustion process, the exhaust feeding period must be designed accordingly. For example, in one set of experiments carried out in the ILMARI facility (Tiitta et al. 2016) the study design was to cover the following phases of the sequential batches of wood logs; ‘cold ignition’, flaming combustion, residual char burning and ‘hot ignition’. In the experiments, a middle-European type modern chimney stove (model: Aduro 9.3) fired with dry spruce logs was used as the emission source, and the first batch of wood logs (2.5 kg) was ignited from the top by using sticks of the same wood (0.25 kg) as kindling, and combusted until the residual char burning phase (for 35 min). The sequential batch of wood logs was then ignited by adding the batch on top of the glowing char residue. In this set of experiments, the whole first batch from ‘cold start’ was injected into the chamber, but it is also possible to inject emissions from any of the above-mentioned burning phases or several of them, depending on the desired aerosol to be studied.

In experiments utilizing pellet boiler emissions with a continuous burning process, a variable feeding time can be used to achieve the desired particle concentration. It is

**Fig. 5.15** SOA yield as a function of seed surface area using either ammonium sulphate seed or pellet-burning primary aerosol as a seed



recommended that the pellet boiler is operated at its nominal load for at least one hour before injection in order to let the combustion process and emission characteristics stabilize, unless ‘cold start’ burning is to be studied. In pellet boilers, different kinds of pellets from different woods can be burned by simply loading them into the boiler. Typical wood pellet boilers utilize a device that automatically loads pellets into the fire at a prescribed rate, as shown in Heringa et al. (2012).

The choice of wood stove can depend on the objectives of the study. For instance, in the PSI chamber, three wood stoves were used to probe the formation of SOA from wood combustion (Stefenelli et al. 2019). In this study, 2–3 kg of beech wood was loading into the selected stove and the fire was started with a mixture of paraffin and wood shavings. Flaming and smouldering phases of the fire were investigated. Typically for the smouldering phase the fire was allowed to proceed and the air intake reduced to cool the fire, which transitioned into a smouldering burning phase coupled with a white smoke exhaust. To generate a continuous flaming phase the stove was operated in a high airflow mode to keep flames visible. The emissions were injected into the atmospheric simulation chamber after passing them through a Dekati ejector dilution stage, which dilutes the emissions with purified air at a ratio of 10:1. A final dilution ratio of 100–200:1 was achieved in the chamber. The lines from the stove and the Dekati ejector were all heated to 150 °C to ensure all emissions were injected into the chamber and limit the losses of semi-volatiles and intermediate volatility species. After the emissions were injected, several minutes (5–20 min.) were allowed for the contents of the chamber to equilibrate.

### *Vehicles and engines*

In vehicle emission studies, a variety of engine conditions can be probed depending on the equipment available in each facility. These studies can range from vehicle idling, constant speeds (torque or power), or simulated driving conditions. The studies that are possible depend on the availability and type of a dynamometer. If driving cycles cannot be performed at simulation chamber facilities, portable chambers or dynamometers can be temporarily installed, as described by Platt et al. (2013, 2017).

Engines mounted in a test rig can be used in chamber studies. As mentioned above, the types of experiments will depend on the capability of the test rig and can be conducted using constant or varying engine operation parameters. Here follows the description of a general protocol for coupling the emissions from various engines to atmospheric simulation chambers, adapted from Platt et al. (2013, 2017), and Pereira et al. (2018).

An example experimental set-up from the University of Manchester is provided in Fig. 5.16. The warm-up time of the engine depends significantly on the type of emissions to be studied (cold start, constant operational conditions, or standard driving cycles). For instance, if cold start experiments are the aim of the study then there will be no significant preparation of the engine. Injections of cold start emissions into the atmospheric simulation chamber must occur on a very fast time scale, within the first 60 s of starting the engine. This time scale ensures the engine and after-treatment systems are not sufficiently warm and will capture most of the VOCs that are emitted. On the other hand, if constant conditions or driving cycles are desired

then a warm-up time will be necessary and this will vary according to engine type. However, in general, the warm-up time to reach a steady temperature in the engine is  $\sim 10$  min. After the warm-up time has lapsed, the emissions can be injected into the chamber for as long as required, depending on the aim of the study.

Depending on the study design, the emission can be diluted before injecting it into the chamber, or the emission can be injected directly into the chamber. The latter procedure can be used in cases where rapid changes in driving or combustion conditions take place (e.g. standard driving cycles), however, it is not exclusively used in these circumstances (see Platt et al. 2017). In typical chamber experiments with combustion exhaust in ILMARI, the sample is diluted in a two-stage dilution system with purified air at room temperature (Fig. 5.17), and the total dilution ratio (DR) is determined by measuring the  $\text{CO}_2$  concentration in the raw emission and in the chamber. One requirement is that the sample transport line before the dilution system is heated to  $150\text{--}250^\circ\text{C}$ , depending on the temperature at the sampling point. It is also recommended that the sample transport line between the first and second diluter is heated to approximately  $80\text{--}120^\circ\text{C}$  in order to avoid condensation and thermophoretic sample losses.

If the emission is injected directly into the chamber, the best practice procedures for the transfer of engine emissions into a reaction chamber include:

- Use of a high flow ( $0.1\text{--}3\text{ m}^3\text{ min}^{-1}$ ) of clean air to mix and dilute the engine emissions into the chamber at ambient temperature.
- Introduction of raw exhaust emissions directly into the chamber while cooling and diluting into clean air, which closely represents combustion emissions in the atmosphere.

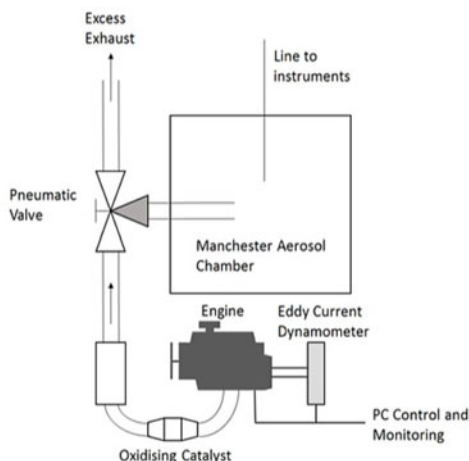


**Fig. 5.16** Schematic of engine injection set-up at the University of Manchester



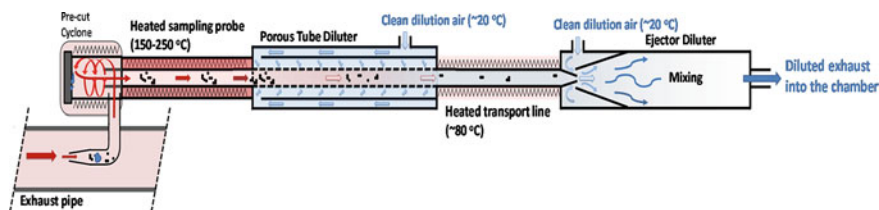


**Fig. 5.17** Schematic of the dilution system at the ILMARI chamber used to inject complex emissions from an engine into the chamber. The emissions first pass through a heated cyclone to remove large particulates, then through a heated sampling line to a porous diluter to dilute the emission by up to a factor of 10. The diluted emissions pass through a second dilution stage and into the chamber at high flow rates ( $\sim 0.1\text{--}3\text{ m}^3\text{ min}^{-1}$ ). Figure by Olli Sippula, UEF

To verify that the gas phase emissions have been effectively transferred to the atmospheric simulation chamber, a comparison of the emissions directly from the source engine should be compared to the gas phase concentrations in the chamber. This can be accomplished by comparing the normalized  $\text{CO}_2$  concentrations to other relevant measured VOCs and total hydrocarbons. For instance, in Platt et al. (2013), the emissions of all relevant gas phase species, including total hydrocarbons, were within 20% of their values directly emitted by the source, thus confirming the effectiveness of the transfer process.

### *Photochemical ageing experiments on combustion emissions*

The current procedure for performing ageing experiments on a combination of exhaust emissions and single precursors in ILMARI is (Kari et al. 2017):

1. Injection of combustion exhaust, either from a single source or from two sources (simultaneous injection).
2. Injection of  $\text{O}_3$  to convert  $\text{NO}$  to  $\text{NO}_2$ , thus enabling a faster start for the photochemistry.
3. Injection of precursor VOC and tracer (e.g. butanol-d9).
4. Injection of oxidant or its precursor ( $\text{HONO}$  or  $\text{H}_2\text{O}_2$  for  $\text{OH}$ , or  $\text{O}_3$ ).
5. Injection of propene or  $\text{NO}_2$ , in order to adjust the VOC-to- $\text{NO}_x$  ratio, if needed.
6. Allow time for stabilization of the injected compounds.
7. Turn the lights on.

The VOC-to- $\text{NO}_x$  ratio depends greatly on the type of sources. For example, in diesel engine exhaust, the VOC-to- $\text{NO}_x$  ratio is typically very low, while in gasoline engine exhaust, the VOC-to- $\text{NO}_x$  ratio is often in the atmospherically relevant range, which enables branching of the different reaction pathways occurring in the atmosphere. The critical values for VOC-to- $\text{NO}_x$  ratio ranging between 3 and 15 have been suggested for the point of 50:50 branching of the reaction pathways (Hoyle et al. 2011, and references therein). The desired VOC-to- $\text{NO}_x$  ratio can be increased by injecting propene or decreased by injecting  $\text{NO}_2$ . It must be noted that if the VOC-to- $\text{NO}_x$  ratio is very low, photochemical oxidation of VOCs is very slow, because the  $\text{OH}$  produced in the chamber is consumed by  $\text{NO}_2$ .

When several emission sources are used, the best practice is to inject the emissions simultaneously, if possible. Simultaneous feeding has been regarded as the best practice in ILMARI because the injection time from a single emission source is relatively long (e.g. 50 min), depending on the desired concentration in the chamber. If the emissions are injected sequentially, the first injected emissions could already start transforming during the injection of the second (and later) emission(s). In ILMARI the simultaneous feeding practice has been used in experiments with emissions from a diesel engine and wood-burning stove.

### 5.5.3 *Plant Emissions*

Due to the importance of biogenic volatile organic compounds (BVOC) for atmospheric chemistry (Guenther 2002) and the large remaining gaps in process-level understanding, BVOC are a subject of continuous research. One concern with investigations of BVOC and their impact on atmospheric chemistry arises from the fact that under natural conditions BVOCs are emitted as complex mixtures, whereas many simulation chamber experiments use single BVOC or simple combinations of BVOC to explore atmospheric chemistry processes. The use of direct emissions from plants is a way of progressing towards more realistic experimental simulations. To improve our understanding on the influence of BVOC emissions on atmospheric processes it is important to be able to study the complex plant emissions from different species under a large variety of different conditions ranging from normal to extreme conditions for the plants. Since BVOC emissions are significantly different between different plant species and can vary significantly with environmental conditions, it is important to have stable environments for the enclosed plants. It is also important to ensure a quantitative and reproducible mechanism for transferring emissions into the simulation chamber so that the complex mixtures and the emission patterns remain unchanged.

#### *Experimental procedure*

The addition of real plant emissions into the atmospheric simulation chamber SAPHIR is achieved by coupling SAPHIR with a PLant chamber Unit for Simulation (PLUS) (Hohaus et al. 2016), Fig. 5.18.

The number of trees needed to reach sufficiently high concentrations in a simulation chamber depends on the volume of the chamber and concentration levels at which users want to work. For experiments to be conducted at atmospheric concentrations of organic compounds in SAPHIR, six trees placed in a sea container beneath the chamber are sufficient. In order to avoid that interactions of the atmosphere with soil influence, the mixture of trace gases that is transferred, the canopies of the trees need to be housed in one Teflon bag (the gas exchange volume), in which emissions of the plants are released. To maximize the transfer and to avoid possible specific compound losses all surfaces inside the gas exchange volume should be chemically inert. In the Jülich chambers, all transfer lines and surfaces are either

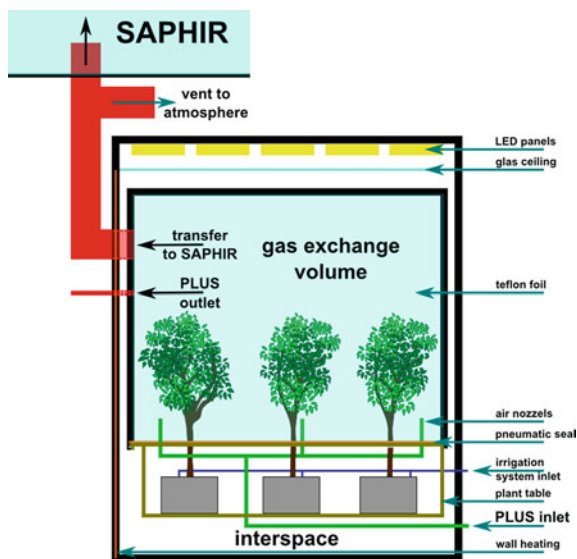


**Fig. 5.18** Schematic of the PLUS plant container as an example of a plant chamber acting as a source for realistic tree emissions. The green lines show the inflow of synthetic air and other gases into PLUS (PLUS inlet) and the red line are the outflows of PLUS to either instrumentation (PLUS outlet), SAPHIR or the atmosphere (Figure reused with permission from Hohaus et al. (2016). Open access under a CC BY 3.0 license, <https://creativecommons.org/licenses/by/3.0>)

made of PFA or have a PFA cover. Also, all cables and connectors inside the gas exchange volume are Teflon-covered. Operation of the plant chamber as a turbulently mixed continuous flow-through reactor is recommended to ensure a homogeneous mixture of plant emissions. Environmental conditions such as light, air and soil humidity,  $\text{CO}_2$  concentrations and temperature in the plant chamber need to be controlled and possibly varied to represent normal or more extreme (e.g. drought) environmental conditions. Tree emissions can be transported using a high flow of air (up to  $30 \text{ m}^3/\text{h}$  for the SAPHIR chamber) in order to reach representative concentrations of organic compounds. It is recommended that the ingoing and outgoing flows are continuously monitored to access potential leakage and the outgoing flow is measured contactless with an ultra-sonic flowmeter. Plant conditions and their emissions are recommended to be continuously monitored inside the gas exchange volume by measuring the temperature of the leaves,  $\text{CO}_2$  and water vapour by cavity ring-down spectroscopy (for example, using a CRDS, Picarro, Model G2301, instrument) and emission strength and patterns by, for example, gas chromatography–mass spectrometry (GC–MS) and/or proton reaction mass spectrometry (PTR–MS).

The transfer of organic compounds has been proven to be quantitative by using best practice procedures:

- Use of inert surfaces for the transfer line (PFA).
- Use of a high flow (up to 30 m<sup>3</sup>/h) to minimize the residence time in the transfer line (order of seconds) compared to the residence time of air in the plant chamber (10–50 min).
- Monitoring of the transfer flow rate by an ultra-sonic flowmeter that measures the flow without contact with the air.

### ***Protocol for transfer efficiency and installation and preparation of the plants***

The transfer efficiency of the complete system can be tested using gas standards. As an example, the gas standard used for tests at SAPHIR consisted of acetone, isoprene,  $\alpha$ -pinene, nopinone and methyl salicylate (MeSa) in N<sub>2</sub> (99,999% purity). The compounds should be chosen to represent typical BVOC emissions (isoprene,  $\alpha$ -pinene, MeSa), while also possessing a significant variety in molecular mass, boiling point and solubility in water (see Table 5.2).

The transfer efficiencies between inlet and outlet of the plant chamber and between the plant chamber outlet and simulation chamber inlet can be determined by the ratio of the measured VOC and CO<sub>2</sub> concentration divided by the calculated concentration. Throughout the experiment, the CO<sub>2</sub> can be used as an inert tracer. Relative humidity inside the plant chamber should be varied between 25 and 100% in order to determine any humidity effect on the transmission efficiency. Results of the transfer efficiency as measured for the Jülich chamber are shown in Fig. 5.19. No significant difference in the transfer efficiencies for different VOC can be observed, indicating that within the range of vapour pressure and polarity investigated, the VOC mixtures emitted from trees enclosed in the gas exchange volume are transferred to SAPHIR without changes to the relative composition of the VOC mixture. Transfer is furthermore independent of relative humidity in the range of 25%–100% for both transfer between PLUS inlet and outlet and transfer between PLUS and SAPHIR. VOC mixtures were shown to be quantitatively transferred to SAPHIR, ensuring the emission pattern remains unchanged.

**Table 5.2** Summary of physical and chemical properties of VOC (acetone, isoprene,  $\alpha$ -pinene, nopinone, and methyl salicylate) used in gas standard for transfer efficiency characterization as an example for a suitable mixture of species for testing the transfer efficiency

VOC	Molecular formula	Molar mass	Boiling point (K)
Acetone	C <sub>3</sub> H <sub>6</sub> O	58	329.3
Isoprene	C <sub>5</sub> H <sub>8</sub>	68	307
$\alpha$ -pinene	C <sub>10</sub> H <sub>16</sub>	136	430
Nopinone	C <sub>9</sub> H <sub>14</sub> O	138	482.15
Methyl salicylate	C <sub>8</sub> H <sub>8</sub> O <sub>3</sub>	152	495.2–496.5

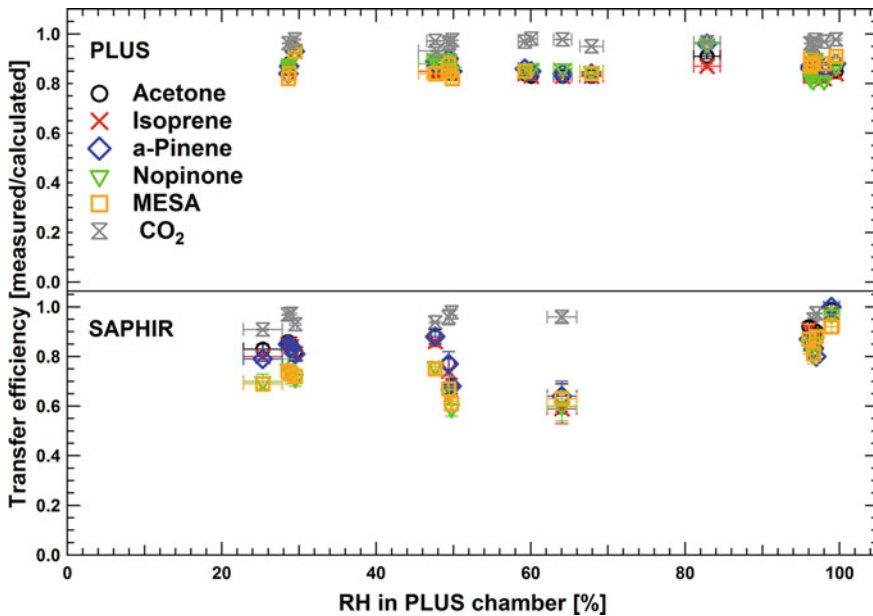


**Fig. 5.19** Example of a test on the transfer efficiency between plant chamber and simulation chamber giving measured/calculated averaged mixing ratios of VOC gas standard compounds. The upper panel shows the transfer efficiency between the Jülich PLUS inlet and PLUS outlet. Lower panel shows the transfer efficiency between PLUS outlet and the SAPHIR chamber. Error bars shown are the standard deviation (NPLUS = 18, NSAPHIR = 37) (Figure reused with permission from Hohaus et al. (2016). Open access under a CC BY 3.0 license, <https://creativecommons.org/licenses/by/3.0>)

Coupling of the plant chamber with the simulation chamber for transfer of BVOC emitted from trees can be achieved by either continuously transferring air from PLUS to SAPHIR or by a short-pulsed coupling (time scale several minutes to hours). For example, Fig. 5.20 displays the temporal evolution of monoterpenes emitted from six *Quercus ilex* trees during transfer of emissions into the SAPHIR chamber. The efficiency of the transfer can be checked by calculating the expected concentration in the simulation chamber from the measured concentrations of organic compounds in the plant chamber and the transfer flow. Apart from the very beginning of the experiment, where calculated concentration of monoterpenes exceeds the observed value, this calculation confirms the high transfer efficiency for the SAPHIR chamber.

Plants should be installed at least 48 h before the start of experiments to allow for the trees to adjust to the new environment. Also, possible changes in the emissions due to damage of leaves or branches during installation need this time to return to normal. Respiration rate, transpiration rate and emission pattern should be monitored. The emission strength of plants is temperature-dependent. This can be tested by

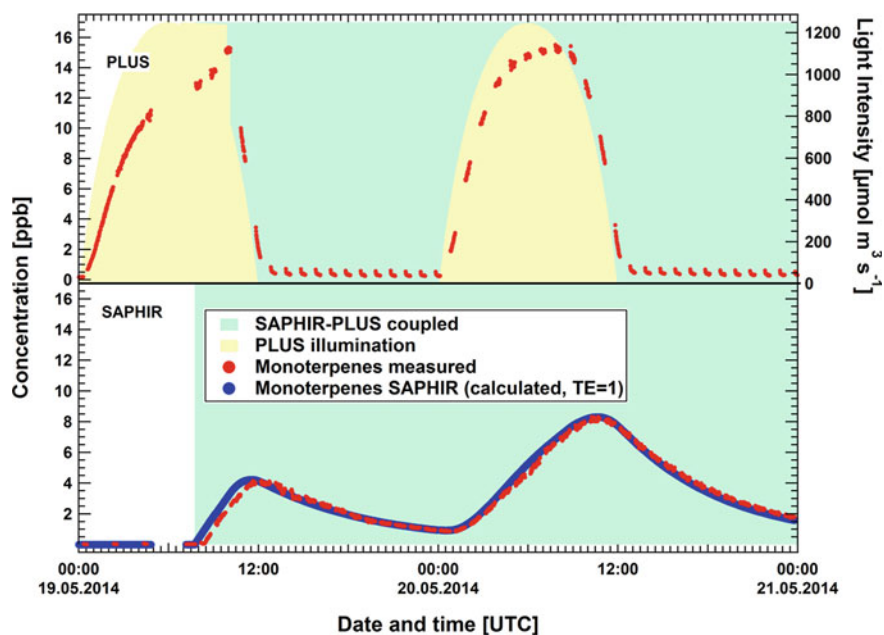


**Fig. 5.20** Illustration of monoterpene transfer from PLUS to SAPHIR when continuously coupling the chambers with a flow of  $30 \text{ m}^3/\text{h}$ . Yellow shaded areas indicate time periods and intensity of light in the plant chamber, green shaded area indicates coupling of PLUS to SAPHIR (Figure reused with permission from Hohaus et al. (2016). Open access under a CC BY 3.0 license, <https://creativecommons.org/licenses/by/3.0>)

measuring the sum of monoterpenes with a PTR-MS for different types of trees (oak and birch) inside the plant chamber. The emission strengths can be also fitted to a parameterization developed by Guenther et al. (1993) as a consistency check. For the SAPHIR chamber, this resulted in a good description for several tested trees, Fig. 5.21.

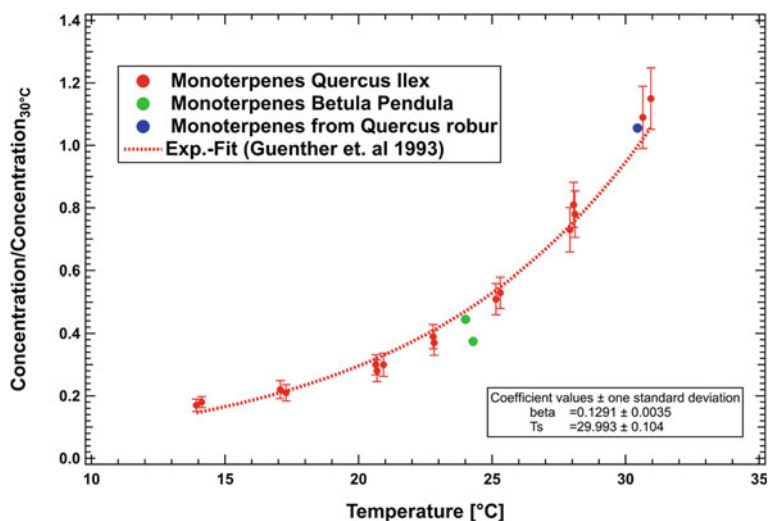


**Fig. 5.21** Relative monoterpene emission strength for two types of oak (*Quercus ilex*, *Quercus robur*) and a birch (*Betula pendula*) with changing temperature of the Jülich plant chamber (Figure reused with permission from Hohaus et al. (2016). Open access under a CC BY 3.0 license, <https://creativecommons.org/licenses/by/3.0>)

## References

- Alsved, M., Bourouiba, L., Duchaine, C., Löndahl, J., Marr, L.C., Parker, S.T., Prussin, A.J., II, Thomas R.J.: Natural sources and experimental generation of bioaerosols: challenges and perspectives. *Aerosol Sci. Technol.* **54**, 547–571 (2019). <https://doi.org/10.1080/02786826.2019.1682509>
- Amato, P., Joly, M., Schaupp, C., Attard, E., Möhler, O., Morris, C.E., Brunet, Y., Delort, A.M.: Survival and ice nucleation activity of bacteria as aerosols in a cloud simulation chamber. *Atmos. Chem. Phys.* **15**, 6455–6465 (2015). <https://doi.org/10.5194/acp-15-6455-2015>
- Baron, P.A., Kulkarni, P. (eds.): *Aerosol Measurement: Principles, Techniques, and Applications*. John Wiley and Sons, West Sussex, UK (2005)
- Baumgardner, D., Popovicheva, O., Allan, J., Bernardoni, V., Cao, J., Cavalli, F., Cozic, J., Diapouli, E., Eleftheriadis, K., Genberg, P.J., Gonzalez, C., Gysel, M., John, A., Kirchstetter, T.W., Kuhlbusch, T.A.J., Laborde, M., Lack, D., Müller, T., Niessner, R., Petzold, A., Piazzalunga, A., Putaud, J.P., Schwarz, J., Sheridan, P., Subramanian, R., Swietlicki, E., Valli, G., Vecchi, R., Viana, M.: Soot reference materials for instrument calibration and intercomparisons: a workshop summary with recommendations. *Atmos. Meas. Tech.* **5**, 1869–1887 (2012). <https://doi.org/10.5194/amt-5-1869-2012>
- Bowers, R.M., McLetchie, S., Knight, R., Fierer, N.: Spatial variability in airborne bacterial communities across land-use types and their relationship to the bacterial communities of potential source environments. *ISME J.* **5**, 601–612 (2011). <https://doi.org/10.1038/ismej.2010.167>
- Brotto, P., Repetto, B., Formenti, P., Panguì, E., Livet, A., Bousserhine, N., Martini, I., Varnier, O., Doussin, J.F., Prati, P.: Use of an atmospheric simulation chamber for bioaerosol investigation: a feasibility study. *Aerobiologia* **31**, 445–455 (2015). <https://doi.org/10.1007/s10453-015-9378-2>
- Bruns, E.A., Krapf, M., Orasche, J., Huang, Y., Zimmermann, R., Drinovec, L., Močnik, G., El-Haddad, I., Slowik, J.G., Dommen, J., Baltensperger, U., révôt, A.S.H.: Characterization of

- primary and secondary wood combustion products generated under different burner loads. *Atmos. Chem. Phys.* **15**, 2825–2841 (2015). <https://doi.org/10.5194/acp-15-2825-2015>
- Caponi, L., Formenti, P., Massabo, D., Di Biagio, C., Cazaunau, M., Pangui, E., Chevallier, S., Landrot, G., Andreae, M.O., Kandler, K., Piketh, S., Saeed, T., Seibert, D., Williams, E., Balkanski, Y., Prati, P., Doussin, J.F.: Spectral- and size-resolved mass absorption efficiency of mineral dust aerosols in the shortwave spectrum: a simulation chamber study. *Atmos. Chem. Phys.* **17**, 7175–7191 (2017). <https://doi.org/10.5194/acp-17-7175-2017>
- Cavalli, F., Viana, M., Yttri, K.E., Genberg, J., Putaud, J.-P.: Toward a standardised thermal-optical protocol for measuring atmospheric organic and elemental carbon: the EUSAAR protocol. *Atmos. Meas. Tech.* **3**, 79–89 (2010). <https://doi.org/10.5194/amt-3-79-2010>
- CH Technologies: Blaustein Atomizer (BLAM) Single-Jet Model—User’s Manual. Westwood, NJ, USA. [https://chtechusa.com/products\\_tag\\_lg\\_blaustein-atomizing-modules-blam.php](https://chtechusa.com/products_tag_lg_blaustein-atomizing-modules-blam.php)
- CH Technologies: Collision Nebulizer—User’s Manual. Westwood, NJ, USA. [https://chtechusa.com/products\\_tag\\_lg\\_collision-nebulizer.php](https://chtechusa.com/products_tag_lg_collision-nebulizer.php)
- CH Technologies: Sparging Liquid Aerosol Generator (SLAG)—User’s Manual. Westwood, NJ, USA. [https://chtechusa.com/products\\_tag\\_lg\\_sparging-liquid-aerosol-slag.php](https://chtechusa.com/products_tag_lg_sparging-liquid-aerosol-slag.php)
- Chiappini, L., Verlhac, S., Aujay, R., Maenhaut, W., Putaud, J.P., Sciare, J., Jaffrezo, J.L., Liousse, C., Galy-Lacaux, C., Alleman, L.Y., Panteliadis, P., Leoz, E., Favez, O.: Clues for a standardised thermal-optical protocol for the assessment of organic and elemental carbon within ambient air particulate matter. *Atmos. Meas. Tech.* **7**, 1649–1661 (2014). <https://doi.org/10.5194/amt-7-1649-2014>
- Chen, H., Navea, J.G., Young, M.A., Grassian, V.H.: Heterogeneous photochemistry of trace atmospheric gases with components of mineral dust aerosol. *J. Phys. Chem. A* **115**, 490–499 (2011). <https://doi.org/10.1021/jp110164j>
- Crawford, I., Möhler, O., Schnaiter, M., Saathoff, H., Liu, D., McMeeking, G., Linke, C., Flynn, M., Bower, K.N., Connolly, P.J., Gallagher, M.W., Coe, H.: Studies of propane flame soot acting as heterogeneous ice nuclei in conjunction with single particle soot photometer measurements. *Atmos. Chem. Phys.* **11**, 9549–9561 (2011). <https://doi.org/10.5194/acp-11-9549-2011>
- Cziczo, D., Froyd, K., Gallavardin, S., Möhler, O., Benz, S., Saathoff, H., Murphy, D.: Deactivation of ice nuclei due to atmospherically relevant surface coatings. *Environ. Res. Lett.* **4**, 044013 (2009). <https://doi.org/10.1088/1748-9326/4/4/044013>
- Danelli, S.G., Brunoldi, M., Massabò, D., Parodi, F., Vernocchi, V., Prati, P.: Comparative characterization of the performance of bio-aerosol nebulizers in connection with atmospheric simulation chambers. *Atmos. Meas. Tech.* **14**, 4461–4470 (2021). <https://doi.org/10.5194/amt-14-4461-2021>
- Després, V., Huffman, J.A., Burrows, S.M., Hoose, C., Safatov, A., Buryak, G., Fröhlich-Nowoisky, J., Elbert, W., Andreae, M., Pöschl, U., Jaenicke, R.: Primary biological aerosol particles in the atmosphere: a review. *Tellus B: Chem. Phys. Meteorol.* **64**, 15598 (2012). <https://doi.org/10.3402/tellusb.v64i0.15598>
- Di Biagio, C., Formenti, P., Styler, S.A., Pangui, E., Doussin, J.F.: Laboratory chamber measurements of the longwave extinction spectra and complex refractive indices of African and Asian mineral dusts. *Geophys. Res. Lett.* **41**, 6289–6297 (2014). <https://doi.org/10.1002/2014gl060213>
- Di Biagio, C., Formenti, P., Balkanski, Y., Caponi, L., Cazaunau, M., Pangui, E., Journet, E., Nowak, S., Caquineau, S., Andreae, M.O., Kandler, K., Saeed, T., Piketh, S., Seibert, D., Williams, E., Doussin, J.F.: Global scale variability of the mineral dust long-wave refractive index: a new dataset of in situ measurements for climate modeling and remote sensing. *Atmos. Chem. Phys.* **17**, 1901–1929 (2017a). <https://doi.org/10.5194/acp-17-1901-2017>
- Di Biagio, C., Formenti, P., Balkanski, Y., Caponi, L., Cazaunau, M., Pangui, E., Journet, E., Nowak, S., Andreae, M.O., Kandler, K., Saeed, T., Piketh, S., Seibert, D., Williams, E., Doussin, J.-F.: Complex refractive indices and single-scattering albedo of global dust aerosols in the shortwave spectrum and relationship to size and iron content. *Atmos. Chem. Phys.* **19**, 15503–15531 (2019). <https://doi.org/10.5194/acp-19-15503-2019>



- Di Biagio, C., Formenti, P., Cazaunau, M., Panguì, E., Marchand, N., Doussin, J.F.: Aethalometer multiple scattering correction Cref for mineral dust aerosols. *Atmos. Meas. Tech.* **10**, 2923–2939 (2017b). <https://doi.org/10.5194/amt-10-2923-2017>
- Engelbrecht, J.P., Moosmüller, H., Pincock, S., Jayanty, R.K.M., Lersch, T., Casuccio, G.: Technical note: Mineralogical, chemical, morphological, and optical interrelationships of mineral dust re-suspensions. *Atmos. Chem. Phys.* **16**, 10809–10830 (2016). <https://doi.org/10.5194/acp-16-10809-2016>
- Ess, M.N., Vasilatou, K.: Characterization of a new mini-CAST with diffusion flame and premixed flame options: Generation of particles with high EC content in the size range 30 nm to 200 nm. *Aerosol Sci. Technol.* **53**, 29–44 (2019). <https://doi.org/10.1080/02786826.2018.1536818>
- Formenti, P., Rajot, J.L., Desboeufs, K., Saïd, F., Grand, N., Chevaillier, S., Schmechtig, C.: Airborne observations of mineral dust over western Africa in the summer Monsoon season: spatial and vertical variability of physico-chemical and optical properties. *Atmos. Chem. Phys.* **11**, 6387–6410 (2011). <https://doi.org/10.5194/acp-11-6387-2011>
- Fröhlich-Nowoisky, J., Pickersgill, D.A., Després, V.R., Pöschl, U.: High diversity of fungi in air particulate matter. *Proc. Natl. Acad. Sci.* **106**, 12814–12819 (2009). <https://doi.org/10.1073/pnas.0811003106>
- Guenther, A.: The contribution of reactive carbon emissions from vegetation to the carbon balance of terrestrial ecosystems. *Chemosphere* **49**, 837–844 (2002). [https://doi.org/10.1016/S0045-6535\(02\)00384-3](https://doi.org/10.1016/S0045-6535(02)00384-3)
- Guenther, A.B., Zimmerman, P.R., Harley, P.C., Monson, R.K., Fall, R.: Isoprene and monoterpene emission rate variability: model evaluations and sensitivity analyses. *J. Geophys. Res.: Atmos.* **98**, 12609–12617 (1993). <https://doi.org/10.1029/93JD00527>
- Haller, T., Rentenberger, C., Meyer, J.C., Felgitsch, L., Grothe, H., Hitznerberger, R.: Structural changes of CAST soot during a thermal–optical measurement protocol. *Atmos. Meas. Tech.* **12**, 3503–3519 (2019). <https://doi.org/10.5194/amt-12-3503-2019>
- Healy, D., O’Connor, D., Sodeau, J.: Measurement of the particle counting efficiency of the “Waveband Integrated Bioaerosol Sensor” model number 4 (WIBS-4). *J. Aerosol Sci.* **47**, 94–99 (2012a). <https://doi.org/10.1016/j.jaerosci.2012.01.003>
- Healy, D.A., O’Connor, D.J., Burke, A.M., Sodeau, J.R.: A laboratory assessment of the Waveband Integrated Bioaerosol Sensor (WIBS-4) using individual samples of pollen and fungal spore material. *Atmos. Environ.* **60**, 534–543 (2012b). <https://doi.org/10.1016/j.atmosenv.2012.06.052>
- Heringa, M.F., DeCarlo, P.F., Chirico, R., Lauber, A., Doberer, A., Good, J., Nussbaumer, T., Keller, A., Burtscher, H., Richard, A., Miljevic, B., Prevot, A.S.H., Baltensperger, U.: Time-resolved characterization of primary emissions from residential wood combustion appliances. *Environ. Sci. Technol.* **46**, 11418–11425 (2012). <https://doi.org/10.1021/es301654w>
- Hohaus, T., Kuhn, U., Andres, S., Kaminski, M., Rohrer, F., Tillmann, R., Wahner, A., Wegener, R., Yu, Z., Kiendler-Scharr, A.: A new plant chamber facility, PLUS, coupled to the atmosphere simulation chamber SAPHIR. *Atmos. Meas. Tech.* **9**, 1247–1259 (2016). <https://doi.org/10.5194/amt-9-1247-2016>
- Hoyle, C.R., Boy, M., Donahue, N.M., Fry, J.L., Glasius, M., Guenther, A., Hallar, A.G., Huff Hartz, K., Petters, M.D., Petäjä, T., Rosenoern, T., Sullivan, A.P.: A review of the anthropogenic influence on biogenic secondary organic aerosol. *Atmos. Chem. Phys.* **11**, 321–343 (2011). <https://doi.org/10.5194/acp-11-321-2011>
- Hoyle, C.R., Fuchs, C., Järvinen, E., Saathoff, H., Dias, A., El Haddad, I., Gysel, M., Coburn, S.C., Tröstl, J., Bernhammer, A.K., Bianchi, F., Breitenlechner, M., Corbin, J.C., Craven, J., Donahue, N.M., Duplissy, J., Ehrhart, S., Frege, C., Gordon, H., Höppel, N., Heinritzi, M., Kristensen, T.B., Molteni, U., Niehman, L., Pinterich, T., Prévôt, A.S.H., Simon, M., Slowik, J.G., Steiner, G., Tomé, A., Vogel, A.L., Volkamer, R., Wagner, A.C., Wagner, R., Wexler, A.S., Williamson, C., Winkler, P.M., Yan, C., Amorim, A., Dommen, J., Curtius, J., Gallagher, M.W., Flagan, R.C., Hansel, A., Kirkby, J., Kulmala, M., Möhler, O., Stratmann, F., Worsnop, D.R., Baltensperger, U.: Aqueous phase oxidation of sulphur dioxide by ozone in cloud droplets. *Atmos. Chem. Phys.* **16**, 1693–1712 (2016). <https://doi.org/10.5194/acp-16-1693-2016>

- Hudson, P.K., Gibson, E.R., Young, M.A., Kleiber, P.D., Grassian, V.H.: Coupled infrared extinction and size distribution measurements for several clay components of mineral dust aerosol. *J. Geophys. Res.: Atmos.* **113** (2008a). <https://doi.org/10.1029/2007JD008791>
- Hudson, P.K., Young, M.A., Kleiber, P.D., Grassian, V.H.: Coupled infrared extinction spectra and size distribution measurements for several non-clay components of mineral dust aerosol (quartz, calcite, and dolomite). *Atmos. Environ.* **42**, 5991–5999 (2008b)
- Kari, E., Hao, L., Yli-Pirilä, P., Leskinen, A., Kortelainen, M., Grigonyte, J., Worsnop, D.R., Jokiniemi, J., Sippula, O., Faiola, C.L., Virtanen, A.: Effect of pellet boiler exhaust on secondary organic aerosol formation from  $\alpha$ -Pinene. *Environ. Sci. Technol.* **51**, 1423–1432 (2017). <https://doi.org/10.1021/acs.est.6b04919>
- Kazemimanesh, M., Moallemi, A., Thomson, K., Smallwood, G., Lobo, P., Olfert, J.S.: A novel miniature inverted-flame burner for the generation of soot nanoparticles. *Aerosol Sci. Technol.* **53**, 184–195 (2019). <https://doi.org/10.1080/02786826.2018.1556774>
- Knippertz, P., Stuut, J.B.: *Mineral Dust—A Key Player in the Earth System*. Springer, Dordrecht–Heidelberg–New York–London (2014)
- Kulkarni, P., Baron, P.A., Willeke, K.: *Aerosol Measurement: Principles, Techniques and Applications*. Wiley (2011)
- Kurup, V.P., Shen, H.-D., Banerjee, B.: Respiratory fungal allergy. *Microbes Infect.* **2**, 1101–1110 (2000). [https://doi.org/10.1016/S1286-4579\(00\)01264-8](https://doi.org/10.1016/S1286-4579(00)01264-8)
- Laborde, M., Mertes, P., Zieger, P., Dommen, J., Baltensperger, U., Gysel, M.: Sensitivity of the single particle soot photometer to different black carbon types. *Atmos. Meas. Tech.* **5**, 1031–1043 (2012a). <https://doi.org/10.5194/amt-5-1031-2012>
- Laborde, M., Schnaiter, M., Linke, C., Saathoff, H., Naumann, K.H., Möhler, O., Berlenz, S., Wagner, U., Taylor, J.W., Liu, D., Flynn, M., Allan, J.D., Coe, H., Heimerl, K., Dahlkötter, F., Weinzierl, B., Wollny, A.G., Zannata, M., Cozic, J., Laj, P., Hitzenberger, R., Schwarz, J.P., Gysel, M.: Single particle soot photometer intercomparison at the AIDA chamber. *Atmos. Meas. Tech.* **5**, 3077–3097 (2012b). <https://doi.org/10.5194/amt-5-3077-2012>
- Laborde, M., Crippa, M., Tritscher, T., Jurányi, Z., Decarlo, P.F., Temime-Roussel, B., Marchand, N., Eckhardt, S., Stohl, A., Baltensperger, U., Prévôt, A.S.H., Weingartner, E., Gysel, M.: Black carbon physical properties and mixing state in the European megacity Paris. *Atmos. Chem. Phys.* **13**, 5831–5856 (2013). <https://doi.org/10.5194/acp-13-5831-2013>
- Lafon, S., Alfaro, S.C., Chevaillier, S., Rajot, J.L.: A new generator for mineral dust aerosol production from soil samples in the laboratory: GAMEL. *Aeol. Res.* **15**, 319–334 (2014). <https://doi.org/10.1016/j.aeolia.2014.04.004>
- Laskina O., Young M.A., Kleiber P.D., Grassian V.H.: Infrared extinction spectra of mineral dust aerosol: single components and complex mixtures. *J. Geophys. Res.: Atmos.* **117**, D18210 (2012). <https://doi.org/10.1029/2012JD017756>
- Lee, B., Kim, S., Kim, S.S.: Hygroscopic growth of *E. coli* and *B. subtilis* bioaerosols. *J. Aerosol. Sci.* **33**, 1721–1723 (2002). [https://doi.org/10.1016/s0021-8502\(02\)00114-3](https://doi.org/10.1016/s0021-8502(02)00114-3)
- Leskinen, A., Yli-Pirilä, P., Kuusalo, K., Sippula, O., Jalava, P., Hirvonen, M.R., Jokiniemi, J., Virtanen, A., Komppula, M., Lehtinen, K.E.J.: Characterization and testing of a new environmental chamber. *Atmos. Meas. Tech.* **8**, 2267–2278 (2015). <https://doi.org/10.5194/amt-8-2267-2015>
- Linke, C., Möhler, O., Veres, A., Mohácsi, A., Bozóki, Z., Szabó, G., Schnaiter, M.: Optical properties and mineralogical composition of different Saharan mineral dust samples: a laboratory study. *Atmos. Chem. Phys.* **6**, 3315–3323 (2006)
- Massabò, D., Danelli, S.G., Broto, P., Comite, A., Costa, C., Di Cesare, A., Doussin, J.F., Ferraro, F., Formenti, P., Gatta, E., Negretti, L., Oliva, M., Parodi, F., Vezzulli, L., Prati, P.: ChAMBRé: a new atmospheric simulation chamber for aerosol modelling and bio-aerosol research. *Atmos. Meas. Tech.* **11**, 5885–5900 (2018). <https://doi.org/10.5194/amt-11-5885-2018>
- May, K.R.: The collision nebulizer: description, performance and application. *J. Aerosol Sci.* **4**, 235–243 (1973). [https://doi.org/10.1016/0021-8502\(73\)90006-2](https://doi.org/10.1016/0021-8502(73)90006-2)

- Meyer, N.K., Duplissy, J., Gysel, M., Metzger, A., Dommen, J., Weingartner, E., Alfara, M.R., Fletcher, C., Good, N., McFiggans, G., Jonsson, Å.M., Hallquist, M., Baltensperger, U., Ristovski, Z.D.: Analysis of the hygroscopic and volatile properties of ammonium sulphate seeded and un-seeded SOA particles. *Atmos. Chem. Phys. Discuss.* **8**, 8629–8659 (2008)
- Moallemi, A., Kazemimanesh, M., Corbin, J.C., Thomson, K., Smallwood, G., Olfert, J.S., Lobo, P.: Characterization of black carbon particles generated by a propane-fueled miniature inverted soot generator. *J. Aerosol Sci.* **135**, 46–57 (2019). <https://doi.org/10.1016/j.jaerosci.2019.05.004>
- Mogili, P.K., Kleiber, P.D., Young, M.A., Grassian, V.H.: N<sub>2</sub>O<sub>5</sub> hydrolysis on the components of mineral dust and sea salt aerosol: comparison study in an environmental aerosol reaction chamber. *Atmos. Environ.* **40**, 7401–7408 (2006). <https://doi.org/10.1016/j.atmosenv.2006.06.048>
- Mogili, P.K., Yang, K.H., Young, M.A., Kleiber, P.D., Grassian, V.H.: Environmental aerosol chamber studies of extinction spectra of mineral dust aerosol components: broadband IR-UV extinction spectra. *J. Geophys. Res.: Atmos.* **112** (2007). <https://doi.org/10.1029/2007JD008890>
- Möhler, O., Linke, C., Saathoff, H., Schnaiter, M., Wagner, R., Mangold, A., Krämer, M., Schurath, U.: Ice nucleation on flame soot aerosol of different organic carbon content. *Meteorologische Zeitschrift* **14**, 477–484 (2005a). <https://doi.org/10.1127/0941-2948/2005/0055>
- Möhler, O., Büttner, S., Linke, C., Schnaiter, M., Saathoff, H., Stetzer, O., Wagner, R., Kramer, M., Mangold, A., Ebert, V., Schurath, U.: Effect of sulfuric acid coating on heterogeneous ice nucleation by soot aerosol particles. *J. Geophys. Res.* **110**, D11210 (2005b). <https://doi.org/10.1029/2004JD005169>
- Moore, R.H., Ziemba, L.D., Dutcher, D., Beyersdorf, A.J., Chan, K., Crumeyrolle, S., Raymond, T.M., Thornhill, K.L., Winstead, E.L., Anderson, B.E.: Mapping the operation of the miniature combustion aerosol standard (Mini-CAST) soot generator. *Aerosol Sci. Technol.* **48**, 467–479 (2014). <https://doi.org/10.1080/02786826.2014.890694>
- Moosmüller, H., Engelbrecht, J.P., Skiba, M., Frey, G., Chakrabarty, R.K., Arnott, W.P.: Single scattering albedo of fine mineral dust aerosols controlled by iron concentration. *J. Geophys. Res.:* *Atmos.* **117** (2012). <https://doi.org/10.1029/2011JD016909>
- Pereira, K.L., Dunmore, R., Whitehead, J., Alfara, M.R., Allan, J.D., Alam, M.S., Harrison, R.M., McFiggans, G., Hamilton, J.F.: Technical note: use of an atmospheric simulation chamber to investigate the effect of different engine conditions on unregulated VOC-IVOC diesel exhaust emissions. *Atmos. Chem. Phys.* **18**, 11073–11096 (2018). <https://doi.org/10.5194/acp-18-11073-2018>
- Petzold, A., Ogren, J.A., Fiebig, M., Laj, P., Li, S.-M., Baltensperger, U., Holzer-Popp, T., Kinne, S., Pappalardo, G., Sugimoto, N., Wehrli, C., Wiedensohler, A., Zhang, X.-Y.: Recommendations for reporting “black carbon” measurements. *Atmos. Chem. Phys.* **13**, 8365–8379 (2013). <https://doi.org/10.5194/acp-13-8365-2013>
- Pileci, R.E., Modini, R.L., Bertò, M., Yuan, J., Corbin, J.C., Marinoni, A., Henzing, B., Moerman, M.M., Putaud, J.P., Spindler, G., Wehner, B., Müller, T., Tuch, T., Trentini, A., Zanatta, M., Baltensperger, U., Gysel-Beer, M.: Comparison of co-located refractory black carbon (rBC) and elemental carbon (EC) mass concentration measurements during field campaigns at several European sites. *Atmos. Meas. Tech.* **14**, 1379–1403 (2021). <https://doi.org/10.5194/amt-14-1379-2021>
- Platt, S.M., El Haddad, I., Zardini, A.A., Clairotte, M., Astorga, C., Wolf, R., Slowik, J.G., Temime-Roussel, B., Marchand, N., Ježek, I., Drinovec, L., Močnik, G., Möhler, O., Richter, R., Barmet, P., Bianchi, F., Baltensperger, U., Prévôt, A.S.H.: Secondary organic aerosol formation from gasoline vehicle emissions in a new mobile environmental reaction chamber. *Atmos. Chem. Phys.* **13**, 9141–9158 (2013). <https://doi.org/10.5194/acp-13-9141-2013>
- Platt, S.M., El Haddad, I., Pieber, S.M., Zardini, A.A., Suarez-Bertoa, R., Clairotte, M., Daellenbach, K.R., Huang, R.J., Slowik, J.G., Hellebust, S., Temime-Roussel, B., Marchand, N., de Gouw, J., Jimenez, J.L., Hayes, P.L., Robinson, A.L., Baltensperger, U., Astorga, C., Prévôt, A.S.H.: Gasoline cars produce more carbonaceous particulate matter than modern filter-equipped diesel cars. *Sci. Rep.* **7**, 4926 (2017). <https://doi.org/10.1038/s41598-017-03714-9>

- Ryder, C.L., Highwood, E.J., Rosenberg, P.D., Trembath, J., Brooke, J.K., Bart, M., Dean, A., Crosier, J., Dorsey, J., Brindley, H., Banks, J., Marsham, J.H., McQuaid, J.B., Sodemann, H., Washington, R.: Optical properties of Saharan dust aerosol and contribution from the coarse mode as measured during the Fenec 2011 aircraft campaign. *Atmos. Chem. Phys.* **13**, 303–325 (2013). <https://doi.org/10.5194/acp-13-303-2013>
- Saathoff, H., Naumann, K.H., Schnaiter, M., Schock, W., Möhler, O., Schurath, U., Weingartner, E., Gysel, M., Baltensperger, U.: Coating of soot and  $(\text{NH}_4)_2\text{SO}_4$  particles by ozonolysis products of  $\alpha$ -pinene. *J. Aerosol. Sci.* **34**, 1297–1321 (2003). [https://doi.org/10.1016/S0021-8502\(03\)00364-1](https://doi.org/10.1016/S0021-8502(03)00364-1)
- Schnaiter, M., Gimmler, M., Llamas, I., Linke, C., Jäger, C., Mutschke, H.: Strong spectral dependence of light absorption by organic carbon particles formed by propane combustion. *Atmos. Chem. Phys.* **6**, 2981–2990 (2006). <https://doi.org/10.5194/acp-6-2981-2006>
- Sow, M., Alfaro, S.C., Rajot, J.L., Marticorena, B.: Size resolved dust emission fluxes measured in Niger during 3 dust storms of the AMMA experiment. *Atmos. Chem. Phys.* **9**, 3881–3891 (2009). <https://doi.org/10.5194/acp-9-3881-2009>
- Stefenelli, G., Jiang, J., Bertrand, A., Bruns, E.A., Pieber, S.M., Baltensperger, U., Marchand, N., Aksoyoglu, S., Prévôt, A.S.H., Slowik, J.G., El Haddad, I.: Secondary organic aerosol formation from smoldering and flaming combustion of biomass: a box model parametrization based on volatility basis set. *Atmos. Chem. Phys.* **19**, 11461–11484 (2019). <https://doi.org/10.5194/acp-19-11461-2019>
- Stirnweis, L., Marcolli, C., Dommen, J., Barmet, P., Frege, C., Platt, S.M., Bruns, E.A., Krapf, M., Slowik, J.G., Wolf, R., Prévôt, A.S.H., Baltensperger, U., El-Haddad, I.: Assessing the influence of  $\text{NO}_x$  concentrations and relative humidity on secondary organic aerosol yields from  $\alpha$ -pinene photo-oxidation through smog chamber experiments and modelling calculations. *Atmos. Chem. Phys.* **17**, 5035–5061 (2017). <https://doi.org/10.5194/acp-17-5035-2017>
- Thomas, R.J., Webber, D., Hopkins, R., Frost, A., Laws, T., Jayasekera, P.N., Atkins, T.: The cell membrane as a major site of damage during aerosolization of *Escherichia coli*. *Appl Environ Microbiol* **77**, 920–925 (2011). <https://doi.org/10.1128/aem.01116-10>
- Tiitta, P., Leskinen, A., Hao, L., Yli-Pirilä, P., Kortelainen, M., Grigonyte, J., Tissari, J., Lamberg, H., Hartikainen, A., Kuuspallo, K., Kortelainen, A.M., Virtanen, A., Lehtinen, K.E.J., Komppula, M., Pieber, S., Prévôt, A.S.H., Onasch, T.B., Worsnop, D.R., Czech, H., Zimmermann, R., Jokiniemi, J., Sippl, O.: Transformation of logwood combustion emissions in a smog chamber: formation of secondary organic aerosol and changes in the primary organic aerosol upon daytime and nighttime aging. *Atmos. Chem. Phys.* **16**, 13251–13269 (2016). <https://doi.org/10.5194/acp-16-13251-2016>
- Ullrich, R., Hoose, C., Möhler, O., Niemand, M., Wagner, R., Höhler, K., Hiranuma, N., Saathoff, H., Leisner, T.: A new ice nucleation active site parameterization for desert dust and soot. *J. Atmos. Sci.* **74**, 699–717 (2017). <https://doi.org/10.1175/jas-d-16-0074.1>
- Utry, N., Ajtai, T., Pintér, M., Tombácz, E., Illés, E., Bozóki, Z., Szabó, G.: Mass-specific optical absorption coefficients and imaginary part of the complex refractive indices of mineral dust components measured by a multi-wavelength photoacoustic spectrometer. *Atmos. Meas. Tech.* **8**, 401–410 (2015). <https://doi.org/10.5194/amt-8-401-2015>
- Vlasenko, A., Sjögren, S., Weingartner, E., Gäggeler, H.W., Ammann, M.: Generation of submicron Arizona test dust aerosol: chemical and hygroscopic properties. *Aerosol. Sci. Technol.* **39**, 452–460 (2005). <https://doi.org/10.1080/027868290959870>
- Vlasenko, A., Sjögren, S., Weingartner, E., Stemmler, K., Gäggeler, H.W., Ammann, M.: Effect of humidity on nitric acid uptake to mineral dust aerosol particles. *Atmos. Chem. Phys.* **6**, 2147–2160 (2006). <https://doi.org/10.5194/acp-6-2147-2006>
- Wagner, R., Ajtai, T., Kandler, K., Lieke, K., Linke, C., Müller, T., Schnaiter, M., Vragel, M.: Complex refractive indices of Saharan dust samples at visible and near UV wavelengths: a laboratory study. *Atmos. Chem. Phys.* **12**, 2491–2512 (2012). <https://doi.org/10.5194/acp-12-2491-2012>

- Wang, N., Jorga, S.D., Pierce, J.R., Donahue, N.M., Pandis, S.N.: Particle wall-loss correction methods in smog chamber experiments. *Atmos. Meas. Tech.* **11**, 6577–6588 (2018). <https://doi.org/10.5194/amt-11-6577-2018>
- Ward, D.E., Hardy, C.C.: Smoke emissions from wildland fires. *Environ. Int.* **17**, 117–134 (1991). [https://doi.org/10.1016/0160-4120\(91\)90095-8](https://doi.org/10.1016/0160-4120(91)90095-8)
- Weinzierl, B., Petzold, A., Esselborn, M., Wirth, M., Rasp, K., Kandler, K., SchütZ, L., Koepke, P., Fiebig, M.: Airborne measurements of dust layer properties, particle size distribution and mixing state of Saharan dust during SAMUM 2006. *Tellus B: Chem. Phys. Meteorol.* **61**, 96–117 (2009). <https://doi.org/10.1111/j.1600-0889.2008.00392.x>
- Wu, C., Huang, X.H.H., Ng, W.M., Griffith, S.M., Yu, J.Z.: Inter-comparison of NIOSH and IMPROVE protocols for OC and EC determination: implications for inter-protocol data conversion. *Atmos. Meas. Tech.* **9**, 4547–4560 (2016). <https://doi.org/10.5194/amt-9-4547-2016>
- Yuan, J., Modini, R.L., Zanatta, M., Herber, A.B., Müller, T., Wehner, B., Poulain, L., Tuch, T., Baltensperger, U., Gysel-Beer, M.: Variability in the mass absorption cross section of black carbon (BC) aerosols is driven by BC internal mixing state at a central European background site (Melpitz, Germany) in winter. *Atmos. Chem. Phys.* **21**, 635–655 (2021). <https://doi.org/10.5194/acp-21-635-2021>
- Zangmeister, C.D., Grimes, C.D., Dickerson, R.R., Radney, J.G.: Characterization and demonstration of a black carbon aerosol mimic for instrument evaluation. *Aerosol Sci. Technol.* **53**, 1322–1333 (2019). <https://doi.org/10.1080/02786826.2019.1660302>
- Zhang, X., Cappa, C.D., Jathar, S.H., McVay, R.C., Ensberg, J.J., Kleeman, M.J., Seinfeld, J.H.: Influence of vapor wall loss in laboratory chambers on yields of secondary organic aerosol. *Proc. Natl. Acad. Sci.* **111**, 5802–5807 (2014). <https://doi.org/10.1073/pnas.1404727111>
- Zhen, H., Han, T., Fennell, D.E., Mainelis, G.: A systematic comparison of four bioaerosol generators: affect on culturability and cell membrane integrity when aerosolizing *Escherichia coli* bacteria. *J. Aerosol Sci.* **70**, 67–79 (2014). <https://doi.org/10.1016/j.jaerosci.2014.01.002>

**Open Access** This chapter is licensed under the terms of the Creative Commons Attribution 4.0 International License (<http://creativecommons.org/licenses/by/4.0/>), which permits use, sharing, adaptation, distribution and reproduction in any medium or format, as long as you give appropriate credit to the original author(s) and the source, provide a link to the Creative Commons license and indicate if changes were made.

The images or other third party material in this chapter are included in the chapter's Creative Commons license, unless indicated otherwise in a credit line to the material. If material is not included in the chapter's Creative Commons license and your intended use is not permitted by statutory regulation or exceeds the permitted use, you will need to obtain permission directly from the copyright holder.

